This document is confidential and is proprietary to the American Chemical Society and its authors. Do not copy or disclose without written permission. If you have received this item in error, notify the sender and delete all copies.

The molybdenum-sulfur bond: Electronic structure of low-lying states of MoS.

Journal:	*The Journal of Physical Chemistry*
Manuscript ID	jp-2021-106728.R1
Manuscript Type:	Article
Date Submitted by the Author:	n/a
Complete List of Authors:	Tzeli, Demeter; National and Kapodistrian University of Athens, Department of Chemistry Karapetsas, Ioannis; National and Kapodistrian University of Athens Merriles, Dakota; University of Utah Ewigleben, Joshua ; The University of Utah Morse, Michael; University of Utah, Department of Chemistry

SCHOLARONE™
Manuscripts

The molybdenum-sulfur bond: Electronic structure of low-lying states of MoS.

Demeter Tzeli,[a,b],* Ioannis Karapetsas,[a]

Dakota M. Merriles,[c] Joshua C. Ewigleben,[c] and Michael D. Morse[c],*

[a] Laboratory of Physical Chemistry, Department of Chemistry, National and Kapodistrian University of Athens, Panepistimiopolis Zografou, Athens 157 84, Greece

[b] Theoretical and Physical Chemistry Institute, National Hellenic Research Foundation, 48 Vassileos Constantinou Ave., Athens 116 35, Greece

[c] Department of Chemistry, University of Utah, Salt Lake City, Utah 84112, USA

E-mail: tzeli@chem.uoa.gr, morse@chem.utah.edu

Tel: +30-210-727-4307, +1-801-581-8319

ABSTRACT

The molybdenum-sulfur bond plays an important role in many processes such as nitrogen-fixation and it is found as a building block in layered materials such as MoS_2, known for its various shapes and morphologies. Here, we present an accurate theoretical and experimental investigation of the chemical bonding and the electronic structure of twenty low-lying states of the MoS molecule. Multireference and coupled cluster methodologies, namely MRCISD, MRCISD+Q, RCCSD(T) and RCCSD[T], were employed in conjunction with basis sets up to aug-cc-pwCV5Z-PP/aug-cc-pwCV5Z for the study of these states. We note the significance of including the inner $4s^24p^6$ electrons of Mo and $2s^22p^6$ of S in the correlated space to obtain accurate results. Experimentally, the predissociation threshold of MoS was measured using resonant two-photon ionization (R2PI) spectroscopy, allowing for a precise measurement of the bond dissociation energy (BDE). Our extrapolated computational D_0 value for the ground state is 3.936 eV, in excellent agreement with our experimental measurement of 3.932 ± 0.004 eV. The largest calculated adiabatic D_0 (5.74 eV) and the largest dipole moment (6.50 D) were found for the $^5\Sigma^+$ state, where a triple bond is formed. Finally, the connection of the chemical bonding of the isolated MoS species to the relevant solid, MoS_2, is emphasized. The low-lying septet states of the diatomic molecule are involved in the material as a building block, explaining the stability and the variety of the shapes and morphologies of the material.

I. INTRODUCTION

Transition metal sulfides attract considerable attention because of their widely recognized importance in many biological and industrial processes.[1, 2] The molybdenum-sulfur bond plays an important role in the process of nitrogen-fixation,[3] in the formation of molybdenum-sulfur clusters,[4] in 2D materials,[5] and in many other areas. For instance, MoS_2 forms two-dimensional layers with remarkable mechanical and photoelectric properties,[6] with applications in catalysis, energy conversion and storage, sensing, photonics, nanocomposites, and membranes.[6-10] The diatomic metal sulfides are the simplest systems to understand the metal–sulfur bonding. A thorough understanding of how these species interact is an essential step to increase our knowledge of more complicated systems.

The electronic structure of MoS was calculated in 1989 for the first time by two theoretical groups, by Ma and Dai [11] at the CISD level of theory and by Langhoff *et al.* [12] via the modified coupled pair functional method (MCPF) and the multireference-based state-averaged CASSCF/MRCI methodologies. Both groups used the LANL2DZ basis set for Mo, which includes a relativistic effective core potential for the 28 inner electrons and a [3s,3p,2d] basis set for the 14 outer electrons,[13] and a double [11] or triple [12] zeta quality basis set for S. Ma and Dai calculated four electronic states, $^1\Sigma^+$, $^5\Sigma$, $^5\Pi$, $^1\Sigma^+$;[11] they found the $^1\Sigma^+$ state to be the ground state, while the $^5\Pi$ state was an excited state. On the contrary, Langhoff *et al.* studied seven electronic states, $^5\Pi$, $^3\Delta$, $^5\Sigma^+$, $^3\Pi$, $^5\Delta$, $^7\Pi$, and $^7\Sigma^+$;[12] they calculated the $X^5\Pi$ state to be the ground state. The ground state bond length was calculated as 1.710(1.726) Å at MCPF(MRCI+Q) level, while the MCPF dissociation energy was calculated as D_0 =4.04 eV. The first excited state is a $^3\Delta$ state found at 0.61(0.25) eV at the MCPF(MRCI+Q) level of theory.[12] In 2002 and 2009, the ground $X^5\Pi$ state was studied via DFT(B3LYP and BPW91) using (LANL2DZ and $LANL2DZ_{Mo}$/6-311+G^*_S) basis sets;[14, 15] the DFT r_e and D_e values were calculated as r_e = 2.152-2.163 Å and D_e = 3.43-3.72 eV. Experimentally, the IR spectrum of matrix-isolated MoS was measured[14] and the dissociation energy of the cation, MoS^+, was obtained using guided ion beam tandem mass spectrometry as 3.68±0.05 eV.[16, 17]. Thus, there are four theoretical studies, two of them giving DFT results on the ground state, and all four employed the small basis set, LANL2DZ. Very little experimental data is available. There is a serious gap in the literature for the MoS molecule. The aims of this work are: 1) to fill that gap and 2) to provide useful information regarding the shapes and morphologies of the MoS_2 material adding physical insight in the role of molybdenum-sulfur bond.

Here, accurate data on the ground and low-lying excited states of MoS are provided. Experimentally, the bond dissociation energy (BDE) of the ground state, $X^5\Pi$ is precisely measured using resonant two-photon ionization (R2PI) spectroscopy, while theoretically, the molecule was systematically studied using coupled cluster methodologies, including the core electrons in the valence space for a series of basis sets up to an augmented quintuple weighted core-valence basis set for the calculation of the dissociation energy and bond distance extrapolated to the infinite basis set. Additionally, spectroscopic data, potential energy curves and a bonding analysis of several excited states are provided via high-level multireference configuration interaction methodologies. All these data will be useful in technologically important materials, such as 2D MoS_2 as well as in describing molybdenum containing enzymes.

II. METHODOLOGY

IIA. Computational Details

Twenty low-lying states of MoS are calculated by employing the correlation consistent basis sets of Dunning *et al.*, aug–cc–pV*5*Z, (21s,13p,5d,4f,3g,2h) → [8s,7p,5d,4f,3g,2h] for S,[18] and of Peterson *et al*., aug-cc-pV*5*Z-PP, (17s,14p,12d,5f,4g,3h,2i) → [8s,8p,7d,5f,4g,3h, 2i] for Mo.[19] The latter basis sets employ accurate core relativistic pseudo-potentials for the $1s^2 2s^2 2p^6 3s^2 3p^6$ electrons and treat the $4s^2 4p^6 (5s4d)^6$ electrons of Mo in the *ab initio* calculation. The multireference configuration interaction + single + double excitations (MRCISD),[20] MRCISD+Q[21] where the Davidson correction (+Q) was included in MRCISD, methodology is applied for all states. Additionally, the ground state is also calculated via the restricted coupled cluster + singles + doubles + perturbative triples (RCCSD(T) and RCCSD[T]) methodology.[22] These methods differ in their treatment of the perturbative inclusion of triple excitations. The perturbative triples corrections are computed without contributions of single excitations in the RCCSD[T] method.

Specifically, the ground state, $X^5\Pi$, is systematically studied by employing the C-RCCSD(T) and C-RCCSD[T] methods, in conjunction with a systematic sequence of weighted core correlation consistent Gaussian basis sets ranging from augmented double to augmented quintuple zeta quality, *i.e.*, aug-cc-pwCV*x*Z-PP_{Mo}/aug-cc-pwCV*x*Z_S, *x* = D, T, Q, and 5.[19, 23] These basis sets are designed for the accurate calculation of the correlation of the semi-valence electrons $4s^2 4p^6$ electrons of Mo and $2s^2 2p^6$ of S, which are also included in the valence space of the C-RCCSD(T) method. The size of the basis set ranges from aug-cc-pwCV*DZ*-PP_{Mo}/aug-cc-pwCV*DZ*$_S$: (10s,9p,8d,3f)→[6s,6p,5d,3f] / (14s,10p,3d)→[6s,5p,3d] to aug-cc-pwCV*5Z*-PP_{Mo}/ aug-cc-pwCV*5Z*$_S$: (19s,16p,14d,6f,5g,4h,3i)→[10s,10p,9d,6f,5g,4h,3i] / (21s,13p,9d,7f,5g, 3h)→[12s,11p,9d, 7f,5g,3h]. The complete basis set limit (CBS) of bond distances, dissociation energies and other spectroscopic constants are obtained.

Generally, for the evaluation of the complete basis set limit (CBS) of the energetics, bond distances, spectroscopic values, *etc.* there are two approaches. Approach (I):[24, 25] All parameters are calculated in a series of basis sets and then these obtained values are extrapolated using the exponential formula (2.1), [24, 25] the mixed Gaussian/exponential form (2.2)[24] or the polynomial forms (2.3). [26-27]

$$y_x = y_{CBS} + A\, e^{-Bx}, \qquad (2.1)$$

$$y_x = y_{CBS} + A\, e^{-(x-1)} + B\, e^{-(x-1)^2}, \qquad (2.2)$$

$$y_X = y_{CBS} + \sum_{k=3}^{K} a_k (x + b_k)^{-k} \qquad (2.3)$$

Approach (II):[27-28] the total energies are extrapolated to the CBS limit by (2.1), (2.2) or a simplified form of (2.3),[27-28] e.g., $y_x = y_{CBS} + Ax^{-b}$ (2.4) and then the spectroscopic constants would be defined by the extrapolated CBS PEC. In the present study we use both approaches. First, the CBS limits of bond distances, dissociation energies, and other spectroscopic parameters are calculated employing the exponential form (2.1) via the first approach. Note that this approach has been successfully used as an extrapolation scheme.[25-26] While,

additionally, we use the second approach using the (2.1), (2.2), and (2.4), for the dissociation energy.

For the complete active space self-consistent field (CASSCF) calculations, ten valence electrons are allotted to 9 valence orbitals, *i.e.*, six (5s4d) of Mo + three (3p) orbitals of S. We must keep the $3s^2$ electrons doubled occupied in the CASSCF, because if not, there is a wrong ordering of the orbitals, *i.e.*, the $4p_z^2$ electrons of Mo are incorporated in the active space instead of $3s^2$ of S. The mutual rotation of the orbitals does not alter the ordering. Thus, the $3s^2$ electrons are doubled occupied in the CASSCF but in the following MRCISD calculations, there are also excitations from these orbitals/electrons, *i.e.*, from the 10 valence orbitals. Thus, excitations from the $3s^2$ orbital are also included. The size of the MRCISD spaces is up to 1.1 x 10^9 and it is reduced to about 5 x 10^6 CSFs after applying the internal contraction approximation (icMRCISD).[20] At the RCCSD(T) level of calculations, 12 electrons ($3s^23p^4$ of S and $4d^55s^1$ of Mo) are correlated and the RCCSD(T) space consists of up to 1.2 x 10^6 CSFs, while at the C-RCCSD(T) level, 28 electrons ($2s^22p^63s^23p^4$ of S and $4s^24p^64d^55s^1$ of Mo) are correlated and the C-RCCSD(T) space consists of up to 5 x 10^6 CSFs. Note that in C-RCCSD(T), all electrons are correlated except for $1s^2$ of S and the inner electrons of Mo ($1s^22s^22p^63s^23p^6$), which are treated via accurate core relativistic pseudo-potentials. To evaluate our RCCSD(T), which is a single–reference method, the single (t_1) and the double (t_2) amplitudes and the T_1 diagnostic are checked. It is found that in all calculations the t_1 and t_2 amplitudes were very small. In most cases, they are smaller than 0.05. Moreover, the T_1 diagnostic is about 0.04 or less in all calculations. These small values of t_1 and t_2 amplitudes and of the T_1 diagnostic indicate that the single reference RCCSD(T) and C-RCCSD(T) methods are appropriate for the calculated states of the species. All calculations were done under C_{2v} symmetry constraints, however the CASSCF wave functions possess correct angular momentum symmetry, *i.e.*, $|\Lambda| = 0$ ($\Sigma^{+/-}$), 1 (Π), and 2 (Δ). Thus, Σ^+ corresponds to A_1 symmetry, Σ^- corresponds to A_2, Π is a linear combination of B_1 and B_2, whereas Δ is a linear combination of A_1 and A_2 symmetries. Of course, MRCISD and RCCSD(T) wavefunctions do not display in general pure spatial angular momentum symmetry, but A_1 for Σ^+, A_2 for Σ^-, B_1 or B_2 for Π, and A_1 or A_2 for Δ states.

Potential energy curves (PEC) up to R=15 Å have been plotted at the MRCISD and MRCISD+Q levels of theory for all states. Bond distances, dissociation energies (D_e; adiabatic D_e^a and diabatic D_e^d), relative energy ordering (T_e), and other spectroscopic constants are computed at all of the employed levels of theory. It should be noted that spin-orbit effects are not considered here; hence the calculated states correspond to the Ω-averaged values (J-averaged values for the atomic limits). The scalar relativistic effects are implicitly parametrized in the accurate core relativistic pseudo-potentials that are used here.[23, 29] Moreover, the bonding of the states is analyzed; it is depicted pictorially via a valence bond Lewis (vbL) icons and via 3D contour plots of the valence molecular orbitals.[30] Note that the bond order is the number of chemical bonds between the atoms, *i.e.*, a whole bond corresponds to a pair of electrons, while a half bond corresponds to a bond with one electron. All CASSCF, MRCISD, and RCCSD(T) calculations were carried out with the MOLPRO suite of codes.[31]

IIB. Experimental details

The measurement of the BDE of MoS was conducted using resonant two-photon ionization (R2PI) spectroscopy on the same instrument that was recently used to measure the BDEs of the diatomic lanthanide sulfides and selenides.[32] The spectrometer used in these studies comprises two different chambers, both evacuated to low pressures (10^{-5} – 10^{-6} Torr) and connected by a pneumatic gate valve. The first chamber houses the molecular source. Here, the MoS molecules were produced by pulsed laser ablation (Nd:YAG, 532 nm, 5 ns) of a V:Mo (4:1) alloy disk over which a flow of 40 psig of 0.7% H_2S in helium was pulsed. Collisions between the ablated metal atoms and the H_2S molecules led to the production of the desired MoS molecules. The V:Mo alloy was already available in the laboratory and was the most convenient source of Mo atoms at the time. A pure Mo disk would probably have produced the MoS molecules even more effectively. After the MoS molecules were produced, they continued colliding with the background helium gas, cooling the molecules close to ambient thermal temperatures. Following production and cooling in the reaction channel, the MoS and other molecules exited the terminal orifice of the reaction block, and underwent supersonic expansion into the low-pressure region of the source chamber. In the process, we estimate that the rotational temperature was cooled to below 30 K.[33]

After the molecules exit the terminal orifice, they continue expanding outwardly until they are loosely collimated into a molecular beam by a 1 cm diameter conical skimmer. Upon passage through the skimmer, the molecular beam enters the differentially pumped second chamber, which houses a Wiley-McLaren time-of-flight ion source assembly.[34] Inside the ion source, a pulse of light from an optical parametric oscillator (OPO) laser irradiates the molecular beam. If the wavenumber of the OPO laser matches an optical transition in the molecule, the molecule can be promoted to the excited electronic state. Before the molecule can lose its energy by fluorescence, however, it is irradiated again 25 ns later by a pulse of light from an excimer laser operating on KrF gas (248nm/5.00 eV). The total energy imparted by the two-photon excitation is sufficient to ionize the molecule. Once the molecules are ionized, they are accelerated up the electrode assembly into a time-of-flight mass spectrometer (TOF-MS) and through a reflectron,[35] spatially separating the ions by mass. At the end of the time-of-flight path, the molecules impact a dual microchannel plate (MCP) detector at different times according to their mass (all are singly charged). The temporal resolution of the MCP and the spatial resolution of the Wiley-McLaren electrode assembly allow for mass-resolved optical spectra to be collected as a function of the OPO laser wavelength.

An experimental cycle in our spectrometer begins with the production of the molecule of interest and ends with the digitization of ion signal as the ions impact the MCP. Experimental cycles repeat at a rate of 10 Hz, allowing 10 mass spectra to be collected per second. In these experiments, 30 experimental cycles are averaged at each OPO laser wavelength as the OPO laser scans through a predefined wavelength range in 0.05nm increments. Mass-specific optical spectra are collected by monitoring the signal in a given mass peak as a function of laser wavelength. Further, because of the 25 ns delay between the OPO laser and the KrF laser, all of the peaks in the mass spectrum are doubled, with one peak consisting of ions produced by the absorption of two OPO photons and a second, delayed peak consisting of ions produced by an OPO + KrF

process. Ion signal in the latter peak then displays the spectrum where the upper state survives long enough to be ionized by the KrF laser, 25 ns after the OPO laser is fired. Multiple scans are collected in the energetic vicinity of the predissociation threshold and averaged for the final spectrum. All spectra are calibrated to atomic transitions based on the well-known tabulated atomic energy levels.[36]

In a molecule like MoS, the electronic states at low energies are well-described by the individual potential curves, as calculated in this report. As the ground separated atom limit is approached, however, nonadiabatic and spin-orbit couplings among the multitude of states accessible makes the Born-Oppenheimer approximation invalid. As a result, it becomes fundamentally incorrect to think of the molecule as moving on a single potential energy curve. Couplings among the myriad of states in this high-energy region allow the molecule to hop from curve to curve, eventually finding its way to dissociation if the total energy exceeds the energy of the ground state of the separated atoms. When the dissociation rate is sufficiently fast, the molecule will dissociate before it can be ionized. The purpose of the 25 ns delay between OPO excitation and KrF ionization is to allow sufficient time for molecules excited above the ground separated atom limit to dissociate. Although the predissociation threshold that is observed represents an upper limit to the BDE of the molecule, there is good reason to believe that in systems with a high density of electronic states, efficient predissociation occurs as soon as the BDE is exceeded in energy.[37-39] Thus, the observed predissociation threshold provides a good estimate of the true thermochemical BDE.

III. RESULTS AND DISCUSSION

III.1. Experimental Section

The R2PI spectrum of MoS in the vicinity of its predissociation threshold is exhibited in Figure 1. Here, the predissociation threshold is given as the point at which the complicated quasicontinous spectrum of vibronic transitions falls to baseline. In Figure 1, the top blue trace is the $^{98}Mo^{32}S^+$ ion signal, with an arrow pointing to where the predissociation threshold in MoS is assigned, at 31 715(30) cm^{-1} (3.932(4) eV). At the top of the arrow is an overhanging bar, which visually defines the 30 cm^{-1} error limit assigned to the BDE of MoS. This error limit was assigned to account for various experimental uncertainties: the rotational temperature of the molecules (~20 cm^{-1}), the linewidth of the OPO laser in this energy range (<10cm^{-1}), and a subjective assessment of the sharpness of the predissociation threshold. The red trace at the bottom of the figure displays the Mo atomic transitions that were recorded simultaneously with the MoS molecular signal. These were used to calibrate the wavenumber axis of the MoS spectrum. The MoS spectrum also displays a few sharp decreases in intensity that fall at the same wavenumbers as the strong Mo atomic lines (near 31 300 and 31 533 cm^{-1}). These are artifacts resulting from the huge number of Mo^+ atomic ions produced at these wavenumbers. The large number of Mo^+ atomic ions produced on resonance causes the entire ion cloud to expand as it traverses the time-of-flight drift tube so that only a small fraction of the ions reaches the detector. The number of atomic ions produced is so large that a strong atomic signal is still observed at these wavenumbers, but all other ionic species, including MoS^+, are depleted due to this effect.

III.2. Theoretical Section

The potential energy curves (PECs) of the twenty calculated states of MoS are depicted in Figure 2 and Figure 1S of the supplementary material (SM). The bond distances, dissociation energies, spectroscopic parameters, dipole moments calculated as expectation values ($\langle\mu\rangle$) and by the finite-field method (μ_{FF}) [40, 41] and relative energy differences of the calculated states are given in Table 1. The leading configurations, the formed bonds, the atomic products at the equilibrium position, the asymptotic atomic products, and the avoided crossings that occur are given in Table 2. Below the states are categorized according to their correlated atomic states.

A. States correlated to Mo(^{7}S) + S (^{3}P):

The atomic ground states products of Mo (^{7}S, $5s^14d^5$) and S (^{3}P, $3s^23p^4$) give rise to six molecular states: $^5\Pi$, $^7\Pi$, $^9\Pi$, $^5\Sigma^-$, $^7\Sigma^-$, and $^9\Sigma^-$. Their PECs are plotted in Figure 3 and Figure 2S of the SM. All six states retain the Mo (^{7}S) and S (^{3}P) character in their PECs. The quintets and the septets are bound, while the nonets are repulsive. This happens because in both nonet states, the atoms have their valence electrons, $5s^14d^5$ (Mo) and $3s^23p^4$ (S), with parallel spin; no bonds are formed.

The $X^5\Pi$ state is the ground state, while the $A^5\Sigma^-$, $^7\Pi$, and $^7\Sigma^-$ states lie 1.07, 1.31, and 2.60 eV above the $X^5\Pi$ state. The $X^5\Pi$ and the $^5\Sigma^-$ states have a double bond, $\sigma^2\pi^2$ and $\pi^2\pi^2$ respectively, and their calculated MRCISD+Q/aug-cc-pV5Z(-PP)$_{Mo}$ bond distances are 2.148 and 2.161 Å, respectively. The septets, $^7\Pi$ and $^7\Sigma^-$, have a single bond, *i.e.*, σ^2 and π^2 respectively and as a result their bond distances are elongated by about 0.3 Å. Finally, the vibrational frequencies ω_e are 479($X^5\Pi$), 466($^5\Sigma^-$), 337($^7\Pi$), and 386 cm^{-1} ($^7\Sigma^-$).

B. States correlated to Mo(^{7}S) + S (^{1}D)

The Mo (^{7}S, $5s^14d^5$) + S (^{1}D, $3s^23p^4$) separated atom limit gives rise to three molecular states: $^7\Delta$, $^7\Pi(2)$, and $^7\Sigma^+$. Their PECs are plotted in Figure 4 and Figure 3S of SM. All are bound states. The $^7\Sigma^+$ and $^7\Delta$ states have a half bond, σ^1 and π^1 respectively, and they retain the character Mo (^{7}S) + S (^{1}D) in their PEC. The $^7\Pi(2)$ state presents an avoided crossing with the $^7\Pi(3)$ state that correlates to the excited Mo (^{5}S) + S (^{3}P) limit, thus at r_e the *in situ* atoms, *i.e.*, the atomic states in the minimum, are Mo (^{5}S) + S (^{3}P) and a σ^2 bond is formed. The MRCISD+Q r_e and D_e values for dissociation to the ^{7}S + ^{1}D limit are 2.376 Å, 2.50 eV ($^7\Sigma^+$), 2.451 Å, 1.94 eV ($^7\Delta$), and 2.538 Å, 1.83 eV ($^7\Pi(2)$). The diabatic D_e value for the $^7\Pi(2)$ state with respect to the *in situ* atoms (^{7}S + ^{1}D) is 2.04 eV.

C. States correlated to Mo(^{5}S) + S (^{3}P):

Totally, six states result from the Mo (^{5}S, $5s^14d^5$) + S (^{3}P, $3s^23p^4$) separated atom limit: $a^3\Sigma^-$, $^3\Pi$, $^5\Pi(2)$, $^5\Sigma^-(2)$, $^7\Pi(3)$, and $^7\Sigma^-(2)$, see Figure 5 and 4S of SM. The Mo atom is excited; the Mo (^{5}S, $5s^14d^5$) ← Mo (^{7}S, $5s^14d^5$) energy difference is calculated as 1.354(1.271) eV at the MRCISD(MRCISD+Q)/aug-cc-pV5Z level,

in excellent agreement with the experimental value of 1.335 eV.[36] Five of these states are bound, while the $^7\Sigma^-(2)$ state is repulsive. Finally, the $a^3\Sigma^-$, $^5\Sigma^-(2)$, and $^7\Pi(3)$ states present avoided crossings with the $^3\Sigma^-(2)$, $^5\Sigma^-(3)$, and $^7\Pi(2)$ states, respectively, see Table 3.

The first excited state of MoS is the $a^3\Sigma^-$ state which is located 0.59 eV above the $X^5\Pi$ state. It is of interest that the first excited state $a^3\Sigma^-$ presents an avoided crossing at 3.2 Å with another $^3\Sigma^-(2)$ state and as a result the $a^3\Sigma^-$ state changes its character to Mo(^{5}D) + S (^{3}P). The diabatic and adiabatic curves of the $a^3\Sigma^-$ state are depicted in Figure 5. This state has a triple bond, $\sigma^2\pi^2\pi^2$, and the shortest bond distance r_e = 2.070 Å at the MRCISD+Q/aug-cc-pV5Z(-PP)$_{Mo}$ level of theory. Its corresponding adiabatic D_e value (dissociation to $^5S + ^3P$) is 4.375 eV, while the diabatic D_e (dissociation to $^5D + ^3P$) is 4.740 eV. Finally, its vibrational frequency is 555 cm^{-1}; this state has the largest harmonic frequency among all of the calculated states.

The $^5\Sigma^-(2)$ state also present an avoided crossing at ~3 Å with a $^5\Sigma^-(3)$, which correlates to the Mo(^{5}D) + S (^{3}P) separated atom limit. The $^3\Pi$ and $^5\Sigma^-(2)$ states have a double bond, $\sigma^2\pi^2$, their bond distances are 2.124 and 2.306 Å, and their D_e values (dissociation to $^5S + ^3P$) are 3.819 eV and 2.254 eV, respectively at the MRCISD+Q/aug-cc-pV5Z(-PP)$_{Mo}$ level of theory. The corresponding diabatic D_e (dissociation to $^5D + ^3P$) of $^5\Sigma^-(2)$ is 2.620 eV. The $^5\Sigma^-(2)$ presents a more elongated r_e and smaller D_e values than $^3\Pi$, even though they both form a double bond. These differences result from the fact that the π^2 bond in $^5\Sigma^-(2)$ is dative ($d_{xz}^0 \leftarrow 3p_x^2$) and its σ^2 bond is covalent, while in the $^3\Pi$ state both of its $\sigma^2\,\pi^2$ bonds are covalent. Finally, both $^5\Pi(2)$ and $^7\Pi(2)$ state have a single σ^2 bond, and their MRCISD+Q bond distances and D_e values (dissociation to $^5S + ^3P$) are 2.343 Å, 2.696 eV and 2.538 Å, 1.833 eV, respectively.

D. States correlated to Mo(^{5}D) + S (^{3}P)

Five states have been calculated that correlate to Mo (^{5}D, $5s^24d^4$) + S (^{3}P, $3s^23p^4$): $^5\Sigma^+$, $^3\Delta$, $^5\Delta$, $^3\Sigma^+$, and $^3\Delta(2)$, see Figure 6 and 5S of SM. All are bound states and all present avoided crossings with higher excited states. The $^3\Delta$ state has an avoided crossing with a state that correlates to Mo(^{5}G) + S(^{3}P); the other states have avoided crossings with states that correlate to Mo(^{5}D) + S(^{1}D), see Table 2. All states have a triple $\sigma^2\pi^2\pi^2$ bond. The MRCISD+Q bond distances and the adiabatic(diabatic) dissociation energies are: 2.191 Å, 4.31(5.42) eV for $^5\Sigma^+$; 2.088 Å, 4.27(4.65) eV for $^3\Delta$; 2.164 Å, 3.85(4.96) eV for $^5\Delta$; 2.180 Å, 2.97(4.09) eV for $^3\Sigma^+$; and 2.195 Å, 3.02(4.13) eV for $^3\Delta(2)$. We observe that that the $^3\Delta$ has a shorter bond distance by about 0.1 Å than the remaining four calculated states because its triple bond is formed by a double covalent bond and a single dative bond; the other four states have a single σ^2 covalent and two $\pi^2\pi^2$ dative bonds, see below. The formation of triple bonds results to strong bonds with diabatic dissociation energies up to 5.42 eV ($^5\Sigma^+$).

E. Bonding analysis

The leading configurations, the bonding, the avoided crossings that occur, and the asymptotic and the *in situ* atomic products of the twenty calculated states are given in Table 2. The vbL bonding icons and the electron density of selected states are given in Scheme 1 and Figure 7. These two pictures correspond to the

description of the chemical bonding via the two basic theories, *i.e.*, valence bond (VB) theory and molecular orbital (MO) theory. To compare the two theories, the atomic orbitals with the main contribution are noted for each MO in Fig. 7, while the existent hybridization is discussed below. The vbL icons focus on how the atomic orbitals of the equilibrium atoms are combined to give individual chemical bonds when a molecule is formed, while some of the valence electrons are represented as not shared and not involved in the formation of the molecule. On the contrary, in the MO theory all the electrons of the valence shell are represented as having taken part in the bonding. VB theory is simpler and more convenient than MO for the calculation of the bond order of the diatomics. In MO theory the bond order is half the difference between the number of bonding electrons minus the number of antibonding electrons; however, careful attention must be taken to characterize the orbitals as bonding, antibonding or non-bonding. In the vbL icons, the bond order is the number of chemical bonds between the atoms, *i.e.*, a whole bond corresponds to a pair of electrons, while a half bond corresponds to a bond with one electron. Both theories predict the same bond order after careful examination of the molecular orbitals for the MO theory.

For the bound calculated states of MoS, the bond order ranges from a half bond (σ^1 or π^1) to a triple bond, $\sigma^2\pi^2\pi^2$. The electronic configuration of the ground $X^5\Pi$ state is: $1/\sqrt{2}\{|1\sigma^2 2\sigma^2 3\sigma^1 1\pi_x^2 1\pi_y^2 2\pi_x^1 1\delta_+^1 1\delta_-^1\rangle + 1\sigma^2 2\sigma^2 3\sigma^1 1\pi_x^2 1\pi_y^2\, 2\pi_y^1 1\delta_+^1 1\delta_-^1\rangle]$. According to the vbL icon, this has a double covalent bond σ^2: $4d_{z2}^1$-$3p_z^1$ and π_x^2: $4d_{xz}^1$-$3p_x^1$ (or π_y^2: $4d_{yz}^1$-$3p_y^1$), see Scheme 1. The $1\pi_y^2$ and $2\pi_x^1$ orbitals in B_1 symmetry (or $1\pi_x^2$ and $2\pi_y^1$ in B_2 symmetry) are located mainly on the S and Mo atoms respectively, resulting in a double bond of $\sigma^2\pi^2$. Theoretically, according to the MO theory there are four fully occupied bonding valence orbitals, $1\sigma^2 2\sigma^2 1\pi_x^2 1\pi_y^2$, two half-occupied antibonding orbitals $3\sigma^1 2\pi_x^1$, and two half-occupied non-bonding orbitals $1\delta_+^1 1\delta_-^1$. Thus, the bond could be characterized as a triple bond. However, through examination of the calculated molecular orbitals we observe that the $1\sigma^2$ is mainly on S and $3\sigma^1$ is on Mo and are therefore nonbonding orbitals. Additionally, the $1\pi_x^2$ and $1\pi_y^2$ orbitals of Fig. 6 are an average of the B_1 and B_2 symmetry orbitals. If the calculation is conducting using only one symmetry, B_1 or B_2, then the $1\pi_x^2 2\pi_x^1$ (B_1) or $1\pi_y^2 2\pi_y^1$ (B_2) orbitals are mainly localized on S ($1\pi_x^2$) and Mo ($2\pi_x^1$) in B_1 or on S ($1\pi_y^2$) and Mo ($2\pi_y^1$) in B_2. Thus, they can also be classified as non-bonding orbitals, again giving a bond order of 2. In our discussion below, we calculate the bond order using the vbL picture, because it is more convenient than the MO picture. The second excited state, $^5\Sigma^-$ ($|1\sigma^2 2\sigma^2 3\sigma^1 4\sigma^1 1\pi_x^2 1\pi_y^2 1\delta_+^1 1\delta_-^1\rangle$), also has a double $\pi^2\pi^2$ covalent bond, as do the $^3\Pi$ and $^5\Sigma^-(2)$ states. It may be noted that the bond distance of the calculated states with double bonds ranges from 2.12-2.30 Å.

The first excited state, $a^3\Sigma^-$, which presents an avoided crossing at 3.2 Å with another $^3\Sigma^-(2)$ state, has a triple $\sigma^2\pi^2\pi^2$ bond and the *in situ* atoms are Mo(^{5}D) + S (^{3}P). The two π^2 bonds are covalent, while the σ^2 bond is dative, *i.e.*, $4d_{z2}^0 \leftarrow 3p_z^2$. It should be noted that there is a quite strong hybridization of 3s-3p$_z$ in the molecular orbitals of S, however, the main participant in bonding seems to be the $3p_z^2$. Apart from the $a^3\Sigma^-$ state, triple bonds are formed in the $^5\Sigma^+$, $^3\Delta$, $^5\Delta$, $^3\Sigma^+$, and $^3\Delta(2)$ states. The $^3\Delta$ state also has two π^2 covalent bonds and a σ^2 dative bond, as in the $a^3\Sigma^-$ state, however the *in situ* atoms are Mo(^{5}G) + S (^{3}P) and the main participant in σ^2 bonding seems to be the $3s^2$. The remaining $^5\Sigma^+$, $^5\Delta$, $^3\Sigma^+$, and $^3\Delta(2)$ states form triple bonds with a σ^2 covalent

and two $\pi^2\pi^2$ dative bonds, *i.e.*, $5p_x^0 \leftarrow 3p_x^2$ and $5p_y^0 \leftarrow 3p_y^2$. It is of interest that the Mo 5p orbitals are involved in the bonding; the atomic orbital occupation analysis shows an electron charge of about 0.1 e^-. Bond distances of these states range from 2.07 to 2.20 and the diabatic dissociation energies range from 4.13-5.42 eV at the MRCISD+Q/aug-cc-pV5Z(-PP) level. Finally, the $^7\Pi$, $^7\Sigma^+$, $^5\Pi(2)$, $^7\Sigma^-$, $^7\Delta$, and $^7\Pi(2)$ form a single σ or π bond or a half single bond, their bond distances range from 2.34 -2.54 Å and their diabatic dissociation energies are 1.04-2.70 eV. The lowest energy state forming a single bond is the $^7\Pi$ state, which has a σ^2 covalent bond, *i.e.*, σ^2: $4d_{z2}^1$-$3p_z^1$, see Table 2. Again, there is a quite strong hybridization of 3s-$3p_z$ in molecular orbitals of S, however, the main participant in bonding seems to be the $3p_z$. Finally, it should be noted that in all states, there is a $5s4d_{z2}$ or $5s5p_z4d_{z2}$ hybridization in the molecular orbitals for Mo, which is clearly depicted in MO plots, see Fig. 7.

Comparing the MoS with MoO[38, 42] both have a $X^5\Pi$ ground state, forming double bonds. However, MoO has a bond dissociation energy that is larger by 1.5 eV and a bond distance that is shorter by 0.42 Å than MoS. Specifically, for MoO: expt: D_0 = 5.414(19) eV[38] and calc: D_0 = 5.515±0.007 and r_e = 1.7131±0.0008 at C-RCCSD[T] CBS-limit.[43] This is because S is larger than O and thus the bond distance is increased, resulting in a smaller dissociation energy. Finally, it should be noted that MoS cannot form low-lying states having quadruple bonds as do the neutral and anionic diatomic molecules of Tc, Ru, Rh and Pd, *i.e.*, $TcN^{0/-}$, $RuC^{0/-}$, $RhB,^{0/-}$ and PdBe [44, 45] because the Mo(c^5D; $4d^6$) state is located about 3.156 eV above the Mo(^7S) ground state.[36] Thus, no low-lying states of MoS exist with unoccupied orbitals (5s) that can receive electrons from S resulting in an additional bond beyond the triple bond $\sigma^2\pi^2\pi^2$.

F. Dipole moments

Dipole moments have been calculated as expectation values ($\langle\mu\rangle$) and by the finite-field method (μ_{FF}), see Table 1. Both procedures predict similar values. The difference in the values obtained in the two procedures is less than 0.2 Debye with the exception of the $^5\Delta$, $^5\Pi(2)$, and $^3\Delta(2)$ states. The largest difference is observed for the $^3\Delta(2)$ state, about 1 Debye. It has been reported that the finite-field method is more accurate than expectation values due to fact that the MRCISD methodology is truncated.[44] The ground state $X^5\Pi$ has a dipole moment of 4.71(4.56) Debye at the MRCISD(+Q) level of theory. The largest values are found for the $^5\Sigma^+$ state [6.83(6.50) Debye] and the $^3\Delta(2)$ state [6.50(6.19) Debye], where a single bond, *i.e.*, σ^2 bond is formed. The smallest ones are found for the $^5\Sigma^-$[0.23(0.21) Debye] and $^7\Sigma^-$[0.02(0.23) Debye] states, where $\pi^2\pi^2$ and π^2 bonds are formed, respectively. Generally, we observe that the existence of a σ bond results in large values of the dipole moment, while the existence of doubly π^2 occupied bonds, without any σ bond, results in small values of dipole moments, cf. Table 1 and 2. This occurs because charge is more easily transferred through the σ framework (σ bonds) than through the π framework (π bonds).

Additionally, the occupancy (or not) of the 5s-like 3σ orbital has a major influence on the dipole moment. A major contributing factor to the dipole moment of these sorts of molecules centers on whether the metallic ns-based orbital is occupied (5s for Mo). This orbital is fairly diffuse and polarizable, and projects out on the side of the molecule opposite to the S atom. When it is occupied, it can cancel out some of the polarization

due to the negatively charged S atom. Thus, it would be expected for the largest dipole moments to occur when this orbital is unoccupied, as in the $^5\Sigma^+$ (6.83(6.50) Debye), the $^5\Delta$ (5.040(4.852) Debye), the $^3\Sigma^+$ (5.088(4.789) Debye), and the $^3\Delta(2)$ (6.504(6.191) Debye) states. When this orbital is doubly occupied, it would be expected to give much smaller dipole moments, with examples of $^3\Sigma^-$ (2.697(2.348) Debye) and $^5\Sigma^-(2)$ (1.521(1.871) Debye). When it is singly-occupied, intermediate values might be expected. This is observed for most of the other states, whose dipole moment fall in the range of 2.442(2.098) – 4.938(4.896) Debye, with the exception of the $^7\Sigma^+$ state. However, the $^7\Sigma^+$ state is unique, in that the 2σ orbital is singly occupied. Finally, it also be noted that when the 4σ orbital is occupied, the dipole moments are tiny, as in the $^5\Sigma^-$ (0.234(0.205) Debye), $^7\Sigma^-$ (0.015(0.232) Debye), and $^7\Delta$ (1.267(1.007) Debye) states.

G. Benchmark Calculations for the X^{5}Π state

The importance of the inclusion of the semi-valence electrons $4s^24p^6$ electrons of Mo and $2s^22p^6$ of S in the correlated valence space has been checked. We observe that this inclusion leads to a decrease of about 0.015(0.012) Å in the bond length and an increase in the dissociation energy of about 0.16(0.18) eV at RCCSD(T)(RCCSD[T]) using an augmented quintuple zeta quality basis set, see Table 3.

Moreover, benchmark calculations are carried out for the ground state, $X^5\Pi$. The X state is systematically studied by employing the C-RCCSD(T) and C-RCCSD[T] methods, in conjunction with a series of weighted core correlation consistent basis sets, *i.e.*, aug-cc-pwCVxZ-PP$_{Mo}$/aug-cc-pwCVxZ$_S$, x = D, T, Q, and 5. The semi-valence electrons $4s^24p^6$ electrons of Mo and $2s^22p^6$ of S are also included in the correlated valence space. The extrapolation to the CBS limit of the calculated bond length, dissociation energies (D_e and D_0), and other spectroscopic parameters are depicted in Figure 8 and Figs. 6S-7S of the supplementary material; all calculated values are given in Table 4 and Table 2S of the supplementary material.

The CCSD(T) and CCSD[T] methods differ in their treatment of the perturbative inclusion of triple excitations. They differ in one-fifth order term of the perturbation contribution to the energy, which CCSD(T) includes and CCSD[T] does not.[46-48] While, the CCSD(T) method has been shown to be especially successful for ground-state energies and for the calculation of the properties of systems with single-reference character, it has been reported that CCSD[T] can describe noncovalent interactions better than the CCSD(T), CCSD(TQ), and CCSDT methods comparing to CCSDTQ.[48] Here, we employ both CCSD(T) and CCSD[T] and we compare their results with experimental values.

Two approaches are used for the calculation of the CBS limits. At first, they are obtained using the exponential formula (2.1) on the calculated R_e, D_e, D_0 and ω_e values for the basis sets n =2-5 (Approach I). The CBS limit of the bond distance (R_e) of the $X^5\Pi$ state is calculated as 2.114±0.0005 Å (C-RCCSD(T)) and 2.131±0.001 Å at (C-RCCSD[T]). The CBS limit of the dissociation energy corrected for the zero-point energy is D_0 = 3.78±0.01 eV (C-RCCSD(T)) and 3.956±0.009 eV at (C-RCCSD[T]). We observe that the C-RCCSD(T) methodology predicts a shorter bond length by 0.02 Å, a smaller dissociation energy by 0.18 eV, and smaller harmonic frequency by about 20 cm^{-1} than C-RCCSD[T]; these differences are almost the same at all basis sets. Our experimental dissociation energy is D_0 = 3.932±0.004 eV, in excellent agreement with our

C-RCCSD[T] value. Thus, the C-RCCSD[T] methodology predicts the dissociation energy of the Mo-S diatomic molecule better than C-RCCSD(T). Our best D_e value is 3.99±0.01 (CBS-limit via C-RCCSD[T]), see Table 4. Thus, for a benchmark study of MoS, an augmented weighted core valence quintuple zeta quality basis set is needed where the semi-valence $4s^24p^6$ electrons of Mo and $2s^22p^6$ of S have been included.

Additionally, another extrapolation strategy (Approach II) was applied for the dissociation energy. The CBS limits of D_0 and D_e are obtained using the exponential Eq. (2.1), the mixed Gaussian/exponential Eq. (2.2) and polynomial Eq. (2.4) on the extrapolated total energies, see Table 5 (approach II). We observe that all three extrapolated formulas predict similar dissociation energies. The gap of their values is less than 0.03 eV. Moreover, the CBS limits obtained using the exponential formula (2.1) on the calculated D_e and D_0 values for each basis set (Table 5; approach I) are in excellent agreement with the values obtain with approach II. Thus, both approaches and all three extrapolated forms are very good choices in excellent agreement with the experimental values. From Table 5, it is found that the best choice that exactly predicts our experimental value is the mixed Gaussian/exponential Eq. 2.

It is interesting to note that the bond length, 2.1313 Å at RCCSD(T)/aug-cc-pV5Z(-PP_{Mo}), is almost the same as our best CBS-limit, 2.131±0.001 at C-RCCSD[T]/aug-cc-pwCV5Z(-PP_{Mo}), due to cancellation of errors. Meaning that the elongation of the RCCSD(T) bond distance, since the correlation of the semi-valence Mo and S electrons has not been included, is compensated by the reduction due to the extrapolation to the CBS limit. However, the corresponding D_e or D_0 values are about 0.28 eV smaller than our best CBS-limit showing the importance of the calculation of the semi-valence correlation.

Comparing the bond length and the dissociation energy of the $X^5\Pi$ state obtained at the MRCISD+Q/aug-cc-pV5Z(-$PP)_{Mo}$ level of theory and the CBS limits of the C-RCCSD[T] methodology, we observe that the CBS limits of C-RCCSD[T] predict a shorter bond distance by 0.017 Å and a larger dissociation energy by 0.34 eV. Making these corrections to the results of Table 1, we present in Table 6 our final predicted R_e, D_e, and D_0 values for all twenty calculated states.

H. Mo-S bonding in materials and enzymes

The molybdenum-sulfur bond is found as a building block in layered materials such as MoS_2 known for its various shapes and morphologies.[4, 5] From a crystalline point of view, layered MoS_2 exists in three polymorphic crystalline structures: 1T (tetragonal)[49], 2H (hexagonal),[50] and 3R (rhombohedral), see Figure 9.[51] In the case of mono- to few-layer structures, the 2H-MoS_2 structure is the most thermodynamically stable phase. Furthermore, MoS_2 layered materials are observed to exhibit other morphologies, such as planar[49] and vertically aligned nanosheets[53], nanoflowers,[54] nanotubes,[55] nanowires,[56] and nanoplatelets[57]. Note that the layers are stacked one on top of another, but the bonds between the layers are very weak. This variety of forms could be controlled by choosing suitable synthesis routes and it is feasible to adjust the 2D-MoS_2 properties to develop high performance devices for a variety of applications. In the 1T, 2H and 3R morphologies, each Mo is surrounded by six S atoms, forming single covalent bonds with them, see Figure 9, with bond distances ranging from 2.37 to 2.41 Å[58-60] depending on the conditions; while in other polymorphs the Mo-S bonds range

from 2.38 to 2.59 Å.[61] It is of interest that the septet states of the diatomic MoS form a half or a single bond and they present bond distances ranging in the same region, *i.e.*, they range from 2.36 to 2.52 Å, see Table 6. The lowest septet state, $^7\Pi$, is the fifth excited state of MoS and it is lying 1.3 eV above the ground state. Additionally, the S vacancy of solid MoS_2 has a formation energy of 2.35 eV in S-rich conditions,[62] while the dissociation of the MoS ($^7\Pi$) is 2.66 eV, only 0.3 eV larger. Thus, clearly the septet state of the diatomic molecule is involved in the material as a building block. It is also interesting that the MoS species has bound septet excited states, *i.e.*, $^7\Sigma^+$ and $^7\Delta$, that form a half bond with dissociation energies of 2.82 and 2.26 eV. These values are large given that the bond is formed by only one electron. This can explain the variety of stable morphologies of the material, *i.e.*, it is like carbon, which presents an sp^3 hybridization and forms four bonds, while molybdenum presents an sd^5 hybridization and it can form six bonds.

Additionally, in 2D-MoS_2 and in Mo_xS_y nanoparticles, the Mo-S distances of the surface, when the Mo plane is on the top, are shorter at about 2.3 Å,[63] *i.e.*, up to 0.1 Å with respect to the solid MoS_2 and they resemble the Mo-S bond distances of the quintet states.

Finally, in complexes and in enzymes, Mo atoms are in octahedral coordination forming six bonds,[64-68] with Mo-S bond distances of about 2.35 Å. For instance, in nitrogenase, which is a complex enzyme that catalyzes the formation of ammonia, it is found that the Mo-S bonds have bond distances ranges from 2.31 to 2.35 Å,[68] *i.e.*, similar to the bond distances of the septet states with the shortest bond distances. Note, that in the complexes, Mo is charged and as a result the Mo-S bonds are shorter than in the neutral MoS. In diatomic MoS, the bonds are mainly covalent because the $Mo^+ + S^-$ products are not favored energetically; the first ionization energy of Mo is 7.09243(4) eV[69] and the electron affinity of S is 2.077103(3) eV.[70] Thus, while the $Mo^+(^6S) + S^-(^2P)$ asymptote can yield a $^5\Pi$ state, *i.e.*, the same as the ground state of MoS, these asymptotic products are lying 5.015 eV higher than $Mo(^7S) + S(^3P)$. Of course, in complexes included Mo-S bonds, as in the case of the Fe-S bonds,[71] this energy difference between ionic and covalent bonds can be provided by the interactions with solvent, other ions, ligands, *etc*.

Thus, the data of MoS diatomic molecule could be useful in understanding solid MoS_2 and molybdenum complexes. The connection of an isolated MoS species to the relevant solid, MoS_2 is far from trivial. We hope that the present study and analysis can be of some help for the better understanding of this very interesting material.

IV. CONCLUSION

In this article, we present a detailed and accurate theoretical and experimental investigation of spectroscopic data, potential energy curves, and bonding analysis of twenty low-lying states of the MoS molecule at the highest level of currently achievable accuracy. Theoretically, the states were studied using multireference and coupled cluster methodologies, namely, MRCISD, MRCISD+Q, RCCSD(T) and RCCSD[T], employing the aug-cc-pV*5*Z-PP basis sets. Additionally, the ground state, $X^5\Pi$, was systematically studied using the C-RCCSD(T) and C-RCCSD[T] methods, in conjunction with a series of basis sets aug-cc-

pwCVxZ-PP$_{Mo}$/aug-cc-pwCVxZ$_S$, x = D, T, Q, and 5. Experimentally, for the first time, the predissociation threshold of the MoS has been measured using resonant two-photon ionization spectroscopy, allowing for a precise assignment of the bond dissociation energy.

In contrast to commonly held beliefs, we found that the C-RCCSD[T] methodology predicts the dissociation energy of MoS better than the C-CCSD(T). The C-RCCSD[T] D_0 values are larger by about 5% than the C-RCCSD(T) ones. Our extrapolated D_0 value of the ground state, $X^5\Pi$, is 3.936 eV, is in excellent agreement with our experimental value, 3.932 ± 0.004 eV; the corresponding extrapolated r_e value is 2.131±0.001 Å.

Additionally, we found that the inclusion of the inner $4s^24p^6$ electrons of Mo and $2s^22p^6$ of S in the correlated space is necessary for the accurate calculation of MoS. It results in a shorter bond distance of ~0.02 Å and a larger dissociation energy up to 2 %.

Regarding the bonding, the $X^5\Pi$ ground state has a double covalent bond $\sigma^2\pi^2$, while the first excited state, $a^3\Sigma^-$, has a triple bond $\sigma^2\pi^2\pi^2$. The third excited state $^5\Sigma^+$ also has a triple bond $\sigma^2\pi^2\pi^2$ and presents the largest dissociation energy with respect to the equilibrium atoms, *i.e.*, a diabatic D_0 value of 5.74 eV. The dipole moment of the $X^5\Pi$ state is 4.71(4.56) Debye at the MRCISD(+Q) level of theory, while the largest values are found for the $^5\Sigma^+$[6.83(6.50) Debye] and the $^3\Delta(2)$ states [6.50(6.19) Debye].

Finally, the connection of the chemical bonding of the isolated MoS species to the relevant solid, MoS_2, is emphasized. The low-lying septet states of the diatomic molecule are involved in the material as building blocks. MoS species present a variety of bound septet excited states with significant dissociation energies up to 2.82 eV, even though only a single or a half bond is formed. Like carbon, which presents an sp^3 hybridization forming four bonds, molybdenum presents an sd^5 hybridization forming six bonds involving MoS septet states. The variety of the bound septet states of MoS diatomic explains the variety of the stable morphologies of material.

SUPPORTING INFORMATION

The Supporting Information provided with this article include the spectra shown in Figure 1 in tabular form, along with other files that provide computational results at the CASSCF, MRCISD(+Q), RCCSD(T) and RCCSD[T] levels of theory.

ACKNOWLEDGMENTS

DT acknowledges the National and Kapodistrian University of Athens, Special Accounts for Research Grants for supporting of this research through the project ‘‘SONFM’’ (KE 17034). MDM thanks the National Science Foundation for support of this research under Grant No. CHE-1952924.

AUTHOR DECLARATIONS

Conflict of Interest

The authors have no conflicts to disclose.

DATA AVAILABILITY

The data that support the findings of this study are available within the article and its supplementary material.

REFERENCES

1. Stiefel, E. I.; Matsumoto, K.; Editors, *Transition Metal Sulfur Chemistry: Biological and Industrial Significance. (Symposium held in Honolulu, Hawaii, December 17-22, 1995.) [In: ACS Symp. Ser., 1996; 653]*. 1996; p 358 pp.
2. Hua, M.; Garcia, C. I.; DeArdo, A. J., Precipitation behavior in ultra-low-carbon steels containing titanium and niobium. *Metallurgical and Materials Transactions A: Physical Metallurgy and Materials Science* **1997,** *28A* (9), 1769-1780.
3. Hoffman, B. M.; Lukoyanov, D.; Yang, Z.-Y.; Dean, D. R.; Seefeldt, L. C., Mechanism of nitrogen fixation by nitrogenase: the next stage. *Chem. Rev.* **2014,** *114* (8), 4041-62.
4. Ji, Z.; Trickett, C.; Pei, X.; Yaghi Omar, M., Linking Molybdenum-Sulfur Clusters for Electrocatalytic Hydrogen Evolution. *J. Am. Chem. Soc.* **2018,** *140* (42), 13618-13622.
5. Canton-Vitoria, R.; Tagmatarchis, N.; Sayed-Ahmad-Baraza, Y.; Ewels, C.; Winterauer, D.; Batten, T.; Brunton, A.; Nufer, S., Gas Sensing Using Monolayer MoS_2, Nanoscale Materials for Warfare Agent Detection. In *Nanoscience for Security, NATO Science for Peace and Security Series - A: Chemistry and Biology*, Bittencourt, C.; Ewels, C.; Llobet, E., Eds. Springer: 2017; pp 71-96.
6. Jin, K.; Liu, D.; Tian, Y., Enhancing the interlayer adhesive force in twisted multilayer MoS_2 by thermal annealing treatment. *Nanotechnology* **2015,** *26* (40), 405708/1-405708/7.
7. Bernardi, M.; Palummo, M.; Grossman Jeffrey, C., Extraordinary sunlight absorption and one nanometer thick photovoltaics using two-dimensional monolayer materials. *Nano Lett* **2013,** *13* (8), 3664-70.
8. Krishnan, U.; Kaur, M.; Singh, K.; Kumar, M.; Kumar, A., A synoptic review of MoS_2: Synthesis to applications. *Superlattices Microstruct.* **2019,** *128*, 274-297.
9. Gupta, D.; Chauhan, V.; Kumar, R., A comprehensive review on synthesis and applications of molybdenum disulfide (MoS_2) material: Past and recent developments. *Inorg. Chem. Commun.* **2020,** *121*, 108200.
10. Li, Z.; Meng, X.; Zhang, Z., Recent development on MoS_2-based photocatalysis: A review. *J. Photochem. Photobiol., C* **2018,** *35*, 39-55.
11. Ma, Z.; Dai, S., *Ab initio* studies on the electronic structure of the complexes containing molybdenum-sulfur bond using relativistic effective core potentials. *Acta Chim. Sin. (Engl. Ed.)* **1989,** (3), 201-8.
12. Langhoff, S. R.; Bauschlicher, C. W., Jr.; Pettersson, L. G. M.; Siegbahn, P. E. M., Theoretical spectroscopic constants for the low-lying states of the oxides and sulfides of Mo and Tc. *Chem. Phys.* **1989,** *132* (1-2), 49-58.
13. Hay, P. J.; Wadt, W. R., *Ab initio* effective core potentials for molecular calculations. Potentials for potassium to gold including the outermost core orbitals. *J. Chem. Phys.* **1985,** *82* (1), 299-310.
14. Liang, B.; Andrews, L., Infrared Spectra and Density Functional Theory Calculations of Group 6 Transition Metal Sulfides in Solid Argon. *J. Phys. Chem. A* **2002,** *106* (30), 6945-6951.
15. Sun, X.; Wang, J.; Wu, Z., Chemical Bonding and Electronic Structure of 4d-Metal Monosulfides. *J. Cluster Sci.* **2009,** *20* (3), 525-534.
16. Armentrout, P. B., Guided ion beam studies of transition metal-ligand thermochemistry. *Int. J. Mass Spectrom.* **2003,** *227* (3), 289-302.
17. Cheng, P.; Koyanagi, G. K.; Bohme, D. K., Carbon Disulfide Reactions with Atomic Transition-Metal and Main-Group Cations: Gas-Phase Room-Temperature Kinetics and Periodicities in Reactivity. *J. Phys. Chem. A* **2006,** *110* (8), 2718-2728.
18. Woon, D. E.; Dunning, T. H., Jr., Gaussian basis sets for use in correlated molecular calculations. III. The atoms aluminum through argon. *J. Chem. Phys.* **1993,** *98* (2), 1358-71.
19. Peterson, K. A.; Figgen, D.; Dolg, M.; Stoll, H., Energy-consistent relativistic pseudopotentials and correlation consistent basis sets for the 4d elements Y-Pd. *J. Chem. Phys.* **2007,** *126* (12), 124101.
20. Werner, H. J.; Knowles, P. J., An efficient internally contracted multiconfiguration-reference configuration interaction method. *J. Chem. Phys.* **1988,** *89* (9), 5803-14.
21. Langhoff, S. R.; Davidson, E. R., Configuration interaction calculations on the nitrogen molecule. *Int. J. Quantum Chem.* **1974,** *8* (1), 61-72.
22. Knowles, P. J.; Hampel, C.; Werner, H. J., Coupled cluster theory for high spin, open shell reference wave functions. *J. Chem. Phys.* **1993,** *99* (7), 5219-27.

23. Peterson, K. A.; Dunning, T. H., Accurate correlation consistent basis sets for molecular core–valence correlation effects: The second row atoms Al–Ar, and the first row atoms B–Ne revisited. *J. Chem. Phys.* **2002,** *117* (23), 10548-10560.
24. Schuchardt, K. L.; Didier, B. T.; Elsethagen, T.; Sun, L.; Gurumoorthi, V.; Chase, J.; Li, J.; Windus, T. L., Basis Set Exchange: A Community Database for Computational Sciences. *J. Chem. Inf. Model.* **2007,** *47* (3), 1045-1052.
25. Peterson, K. A.; Woon, D. E.; Dunning, T. H., Benchmark calculations with correlated molecular wave functions. IV. The classical barrier height of the $H+H_2 \rightarrow H_2+H$ reaction. *J. Chem. Phys.* **1994,** *100* (10), 7410-7415.
26. Tzeli, D.; Mavridis, A.; Xantheas, S. S., A first principles study of the acetylene-water interaction. *J. Chem. Phys.* **2000,** *112* (14), 6178-6189.
27. Paizs, B.; Salvador,P.; Császár, A. G.; Duran, M.; Suhai, S. Intermolecular Bond Lengths: Extrapolation to the Basis Set Limit on Uncorrected and BSSE-Corrected Potential Energy Hypersurfaces. *J. Comput. Chem.,* **2001**, *22*, 196–207.
28. Feller, D. Benchmarks of improved complete basis set extrapolation schemes designed for standard CCSD(T) atomization energies. *J. Chem. Phys.* **2013**, *138*, 074103.
29. Varandas, A. J. C. CBS extrapolation of Hartree–Fock energy: People and Dunning basis sets hand-to-hand on the endeavour, Phys. Chem. Chem. Phys., **2019**, *21*, 8022-8034.
30. Tzeli, D.; Mavridis, A., Theoretical investigation of iron carbide, FeC. *J. Chem. Phys.* **2002,** *116* (12), 4901-4921.
31. MOLPRO 2015.1 is a package of ab initio programs written by H.-J. Werner; P. J. Knowles; G. Knizia; F. R. Manby; M. Schütz; P. Celani; W. Györffy; D. Kats; T. Korona; R. Lindh *et al.*
32. Sorensen, J. J.; Tieu, E.; Morse, M. D., Bond dissociation energies of lanthanide sulfides and selenides. *J. Chem. Phys.* **2021,** *154*, 124307.
33. Matthew, D. J.; Morse, M. D., Resonant two-photon ionization spectroscopy of jet-cooled UN: Determination of the ground state. *J. Chem. Phys.* **2013,** *138* (18), 184303.
34. Wiley, W. C.; McLaren, I. H., Time-of-Flight Mass Spectrometer with Improved Resolution. *Rev. Sci. Instrum.* **1955,** *26* (12), 1150 - 1157.
35. Mamyrin, B. A.; Karataev, V. I.; Shmikk, D. V.; Zagulin, V. A., Mass reflectron. New nonmagnetic time-of-flight high-resolution mass spectrometer. *Zh. Eksp. Teor. Fiz.* **1973,** *64* (1), 82-9.
36. Kramida, A.; Ralchenko, Y.; Reader, J.; Team, a. N. A., *NIST Atomic Spectra Database (version 5.7.1)*. National Institute of Standards and Technology, Gaithersburg, MD: 2019.
37. Morse, M. D., Predissociation Measurements of Bond Dissociation Energies. *Acc. Chem. Res.* **2019,** *52*, 119-126.
38. Sorensen, J. J.; Tieu, E.; Sevy, A.; Merriles, D. M.; Nielson, C.; Ewigleben, J. C.; Morse, M. D., Bond dissociation energies of transition metal oxides: CrO, MoO, RuO, and RhO. *J. Chem. Phys.* **2020,** *153*, 074303.
39. Merriles, D. M.; Sevy, A.; Nielson, C.; Morse, M. D., The bond dissociation energy of VO measured by resonant three-photon ionization spectroscopy. *J. Chem. Phys.* **2020,** *153*, 024303.
40. Langhoff, S. R.; Bauschlicher, C. W., Jr.; Partridge, H., Theoretical dipole moment for the $X^2\Pi$ state of NO. *Chem. Phys. Lett.* **1994,** *223* (5-6), 416-22.
41. Tzeli, D.; Mavridis, A., On the dipole moment of the ground state $X^3\Delta$ of iron carbide, FeC. *J. Chem. Phys.* **2003,** *118* (11), 4984-4986.
42. Hamrick, Y. M.; Taylor, S.; Morse, M. D., Optical spectroscopy of jet-cooled MoO. *J. Mol. Spectrosc.* **1991,** *146*, 274-313.
43. Androutsopoulos, A.; Depastas, T.; Tzeli, D., **to be published**.
44. Tzeli, D.; Karapetsas, I., Quadruple Bonding in the Ground and Low-Lying Excited States of the Diatomic Molecules TcN, RuC, RhB, and PdBe. *J. Phys. Chem. A* **2020,** *124* (33), 6667-6681.
45. Tzeli, D., Quadruple chemical bonding in the diatomic anions TcN^-, RuC^-, RhB^-, and PdBe. *J. Comput. Chem.* **2021,** *42* (16), 1126-1137.
46. Urban, M.; Noga, J.; Cole, S. J.; Bartlett, R. J., Towards a full CCSDT model for electron correlation. *J. Chem. Phys.* **1985,** *83* (8), 4041-6.
47. Watts, J. D.; Gauss, J.; Bartlett, R. J., Coupled-cluster methods with noniterative triple excitations for restricted-open-shell-Hartree-Fock and other general single-determinant reference functions. Energies and analytical gradients. *J. Chem. Phys.* **1993,** *98* (11), 8718-33.
48. Řezáč, J.; Šimová, L.; Hobza, P., CCSD[T] Describes Noncovalent Interactions Better than the CCSD(T), CCSD(TQ), and CCSDT Methods. *J. Chem. Theory Comput.* **2013,** *9* (1), 364-9.
49. Xu, H.; Yi, J.; She, X.; Liu, Q.; Song, L.; Chen, S.; Yang, Y.; Song, Y.; Vajtai, R.; Lou, J.; et al. 2D heterostructure comprised of metallic 1T-MoS_2/Monolayer O-g-C_3N_4 towards efficient photocatalytic hydrogen evolution. *Appl. Catal. B Environ.* **2018**, *220*, 379–385.
50. Backes, C.; Berner, N.C.; Chen, X.; Lafargue, P.; LaPlace, P.; Freeley, M.; Duesberg, G.S.; Coleman, J.N.; McDonald, A.R. Functionalization of liquid-exfoliated two-dimensional 2H-MoS_2. *Angew. Chemie - Int. Ed.* **2015**, *54*, 2638–2642.
51. Tan, D.; Willatzen, M.; Wang, Z.L. Prediction of strong piezoelectricity in 3R-MoS_2 multilayer structures. *Nano Energy* **2019**, *56*, 512–515.
52. Yang, P.; Zhang, S.; Pan, S.; Tang, B.; Liang, Y.; Zhao, X.; Zhang, Z.; Shi, J.; Huan, Y.; Shi, Y.; et al. Epitaxial Growth of Centimeter-Scale Single-Crystal MoS_2 Monolayer on Au(111). *ACS Nano* **2020**, *14*, 5036–5045.

53. Chen, X.P.; Xing, G.J.; Xu, L.F.; Lian, H.Q.; Wang, Y. Vertically aligned MoS_2 films prepared by RF-magnetron sputtering method as electrocatalysts for hydrogen evolution reactions. *Compos. Interfaces* **2020**, 1–10.
54. Hu, Z.; Wang, L.; Zhang, K.; Wang, J.; Cheng, F.; Tao, Z.; Chen, J. MoS_2 Nanoflowers with Expanded Interlayers as High-Performance Anodes for Sodium-Ion Batteries. *Angew. Chemie - Int. Ed.* **2014**, *53*, 12794–12798.
55. Chen, J.; Kuriyama, N.; Yuan, H.; Takeshita, H.T.; Sakai, T. Electrochemical hydrogen storage in MoS_2 nanotubes. *J. Am. Chem. Soc.* **2001**, *123*, 11813–11814.
56. Li, W.J.; Shi, E.W.; Ko, J.M.; Chen, Z.Z.; Ogino, H.; Fukuda, T. Hydrothermal synthesis of MoS_2 nanowires. *J. Cryst. Growth* **2003**, *250*, 418–422.
57. Deokar, G.; Vancsó, P.; Arenal, R.; Ravaux, F.; Casanova-Cháfer, J.; Llobet, E.; Makarova, A.; Vyalikh, D.; Struzzi, C.; Lambin, P.; et al. MoS_2–Carbon Nanotube Hybrid Material Growth and Gas Sensing. *Adv. Mater. Interfaces* **2017**, *4*, 1–10.
58. Bell, R.E.; Herfert, R.E. Preparation and characterization of a new crystalline form of molybdenum bisulfide *J. Am. Chem. Soc.* **1957**, *79* 3351-3354.
59. Schonfeld, B.; Huang, J. J.; Moss, S. C. Anisotropic mean-square displacements (MSD) in single crystals of 2H- and 3R-MoS_2 Note: 2H polytype, this is the most common in nature Locality: synthetic *Acta Crystallographica, Section B* **1983**, *39*, 404-407
60. Dickinson, R G; Pauling, L The Crystal Structure of Molybdenite. *J. Am. Chem. Soc.* **1923**, *45* 1466-1471
61. Fukuoka, H.; Masuoka, K.; Hanaoka, T.; Inumaru, K. New Polymorph of Mo_3S_4 Prepared using a High-pressure Synthesis Technique: Crystal Structure, Electronic Property, and Band Calculation *In. Chem.* **2013**, *52*, 7918-7922
62. Liu, D.; Guo, Y.; Fang, L.; Robertson, J. Sulfur vacancies in monolayer MoS_2 and its electrical contacts, *Appl. Phys. Lett.* **2013**, *103*, 183113.
63. Liu, X.; Cao, D.; Yang, T.; Li, H.; Ge, H.; Ramos, M.; Peng, Q.; Dearden, A. K.; Cao, Z.; Yang, Y.; Liag. Y.-W.; Wen, X.-D. Insight into the structure and energy of $Mo_{27}S_xO_y$ clusters, *RSC Adv.*, **2017**, *7*, 9513-9520.
64. Mitchell, P. C. Coordination Compounds of Molybdenum, *Coord. Chem. Rev.* **1966**, *1*, 315-350.
65. Bezdek, M. J.; Guo, S.; Chirik, P. J. Coordination-induced weakening of ammonia, water, and hydrazine X–H bonds in a molybdenum complex, *Science*, **2016**, *354*, 730-733
66. Cordas, C. M.; Moura, J. J. G. Molybdenum and tungsten enzymes redox properties - A brief overview, *Coord. Chem. Rev.,* **2019***, 394*, 53-64
67. Miyagawa, K.; Shoji, M.; Isobe, H.; Yamanaka, S.; Kawakami, T.; Okumura, M.; Yamaguchi, K. Theory of chemical bonds in metalloenzymes XXIV electronic and spin structures of FeMoco and Fe-S clusters by classical and quantum computing, *Mol. Phys.*, **2020**, *118*, 21-22.
68. Bjornsson, R.; Neese, F.; DeBeer, S. Revisiting the Mössbauer Isomer Shifts of the FeMoco Cluster of Nitrogenase and the Cofactor Charge, *In. Chem.* **2017**, *56*, 1470−1477
69. Rayner, D. M.; Mitchell, S. A.; Bourne, O. L.; Hackett, P. A. First-Ionization Potential of Niobium and Molybdenum by Double-Resonance, Field-Ionization Spectroscopy. *J. Opt. Soc. Am. B* **1987**, *4*, 900–905.
70. Chaibi, W.; Peláez, R.J.; Blondel, C.; Drag, C.; Delsart, C. Effect of a magnetic field in photodetachment microscopy. *Eur. Phys. J. D.* **2010**, *58*, 29-37
71. Tzeli, D.; Raugei, D.; Xantheas, S. S. Quantitative Account of the Bonding Properties of a Rubredoxin Model Complex $[Fe(SCH_3)_4]^q$, q = −2, −1, +2, +3. *J. Chem. Theory Comput.* **2021**, *17*, 6080–6091.

Table 1. Bond Lengths r_e (Å), Dissociation Energies D_e (eV), Harmonic Frequencies and Anharmonic Corrections ω_e, $\omega_e x_e$ (cm^{-1}), Rotational Vibrational Couplings α_e (cm^{-1}), Centrifugal Distortions $\overline{D}_e$(cm^{-1}), dipole moments calculated as expectation values ⟨μ⟩ (debye) and by the finite-field method μ_{FF} (debye) and Energy Differences T_e (eV) of twenty calculated states of MoS at the MRCISD, MRCISD+Q, /aug-cc-pV5Z(-PP)$_{Mo}$ level of theory.

State	Method[a]	r_e	D_e	D_e^{d} [a]	ω_e	$\omega_e\chi_e$	$a_e(10^{-4})$	$\overline{D}_e(10^{-8})$	<μ>	μ_{FF}	T_e
***X*^{5}Π**	MRCISD	2.1571	3.371		467.0	2.32	7.663	6.138	4.479	4.710	0.000
	MRCISD+Q	2.1479	3.646		479.0	2.18	7.285	5.986		4.561	0.000
^{3}Σ$^-$	MRCISD	2.0740	4.085	4.486	549.2	1.84	6.396	5.618	2.469	2.697	0.702
	MRCISD+Q	2.0704	4.375	4.740	554.7	1.78	6.285	5.565		2.348	0.594
^{5}Σ$^-$	MRCISD	2.1635	2.393		465.0	1.92	7.094	6.083	0.117	0.234	0.978
	MRCISD+Q	2.1614	2.580		465.8	1.97	7.183	6.095		0.205	1.066
^{5}Σ$^+$	MRCISD	2.1953	4.137	5.292	473.7	1.50	5.484	5.37	7.018	6.829	1.052
	MRCISD+Q	2.1912	4.307	5.422	476.3	1.36	5.299	5.371		6.501	1.027
^{3}Δ	MRCISD	2.0913	4.079	4.338	537.6	1.78	6.343	5.579	3.877	3.965	1.110
	MRCISD+Q	2.0876	4.266	4.654	540.8	1.74	6.264	5.572			1.068
^{7}Π	MRCISD	2.4320	2.162		333.6	1.28	5.859	5.857	4.862	4.938	1.209
	MRCISD+Q	2.4239	2.334		337.1	1.26	5.804	5.852		4.896	1.312
^{3}Π	MRCISD	2.1300	3.559		509.1	1.67	6.08	5.572	4.342	4.436	1.228
	MRCISD+Q	2.1238	3.819		514.5	1.65	6.011	5.551		4.412	1.150
^{5}Δ	MRCISD	2.1692	3.606	4.762	486.0	1.57	5.882	5.479	4.542	5.040	1.583
	MRCISD+Q	2.1642	3.850	4.965	492.4	1.53	5.705	5.413		4.852	1.484
^{7}Σ$^+$	MRCISD	2.3945	2.326		304.2	1.30	6.971	7.733	5.591	5.445	2.201
	MRCISD+Q	2.3759	2.500		313.5	1.35	6.963	7.632		5.059	2.260
^{5}Π(2)	MRCISD	2.3644	2.415		414.2	1.15	3.903	4.498	5.154	4.891	2.372
	MRCISD+Q	2.3427	2.696		406.8	1.73	3.231	4.929		4.667	2.273
^{3}Σ$^+$	MRCISD	2.1917	2.733	3.888	437.9	2.79	8.211	6.347	4.857	5.088	2.456
	MRCISD+Q	2.1797	2.973	4.087	457.0	2.48	7.283	6.023		4.789	2.362
^{3}Δ(2)	MRCISD	2.2158	2.682	3.838	443.8	2.22	5.808	5.786	5.454	6.504	2.506
	MRCISD+Q	2.1954	3.017	4.132	468.7	1.80	4.904	5.481		6.191	2.317
^{7}Σ$^-$	MRCISD	2.3824	0.812		384.0	2.26	5.066	5.002	0.184	0.015	2.559
	MRCISD+Q	2.3944	1.043		386.0	1.02	3.38	4.805		0.232	2.603
^{7}Δ	MRCISD	2.4578	1.791		326.8	0.92	4.969	5.728	1.45	1.267	2.736
	MRCISD+Q	2.4511	1.935		328.3	0.95	5.084	5.769		1.007	2.825
^{5}Σ$^-$(2)	MRCISD	2.3185	1.957	2.358	384.4	0.97	5.43	5.876	0.252	1.521	2.831
	MRCISD+Q	2.3065	2.254	2.620	387.5	1.04	5.704	5.967		1.871	2.714
^{7}Π(2)	MRCISD	2.5487	1.684	1.945	310.8	0.88	4.303	5.093	3.008	2.501	2.843
	MRCISD+Q	2.5380	1.833	2.042	308.6	0.93	4.528	5.297		2.146	2.927
^{7}Π(3)	MRCISD	2.5328	1.428		307.2	0.95	4.936	5.413	2.509	2.442	3.382
	MRCISD+Q	2.5232	1.501		308.9	0.98	5.092	5.476		2.098	3.474
^{9}Σ$^-$	MRCISD		repulsive								3.361
	MRCISD+Q		repulsive								3.647
^{9}Π	MRCISD		repulsive								3.371
	MRCISD+Q		repulsive								3.646
^{7}Σ$^-$(2)	MRCISD		repulsive								4.788
	MRCISD+Q		repulsive								4.969

[a] D_e^{d}: Diabatic dissociation energy.

Table 2. Leading Configurations, Bonding, Atomic products at r_e,[a] bond distances (Å) where Avoided Crossings occur, and Asymptotic atomic products[a] (15 Å) at the MRCISD/aug-cc-pV5Z(-PP)$_{Mo}$ level of theory

State	Leading configuration (valence electrons)	Bonds	Atomic products at r_e	Avoid. Cross.	Asymptotic atomic products
$X^5\Pi$	$\frac{0.89}{\sqrt{2}}\left\|1\sigma^2 2\sigma^2 3\sigma^1\left(1\pi_x^2 1\pi_y^2 2\pi_y^1 + 1\pi_x^2 2\pi_x^1 1\pi_y^2\right)1\delta_+^1 1\delta_-^1\right\rangle)$	$\sigma^2\pi^2$	Mo(^{7}S) + S(^{3}P)	-	Mo(^{7}S) + S(^{3}P)
$^3\Sigma^-$	$0.89\|1\sigma^2 2\sigma^2 3\sigma^2 1\pi_x^2 1\pi_y^2 1\delta_+^1 1\delta_-^1\rangle$	$\sigma^2\pi^2\pi^2$	Mo(^{5}D) + S(^{3}P)	3.2	Mo(^{5}S) + S(^{3}P)
$^5\Sigma^-$	$0.88\|1\sigma^2 2\sigma^2 3\sigma^1 4\sigma^1 1\pi_x^2 1\pi_y^2 1\delta_+^1 1\delta_-^1\rangle$	$\pi^2\pi^2$	Mo(^{7}S) + S(^{3}P)	-	Mo(^{7}S) + S(^{3}P)
$^5\Sigma^+$	$0.96\|1\sigma^2 2\sigma^2 1\pi_x^2 2\pi_x^1 1\pi_y^2 2\pi_y^1 1\delta_+^1 1\delta_-^1\rangle$	$\sigma^2\pi^2\pi^2$	Mo(^{5}D) + S(^{1}D)	3.0	Mo(^{5}D) + S(^{3}P)
$^3\Delta$	$0.91\|1\sigma^2 2\sigma^2 3\sigma^1 1\pi_x^2 1\pi_y^2\left(1\delta_+^1 1\delta_-^2 + 1\delta_+^2 1\delta_-^1\right)\rangle$	$\sigma^2\pi^2\pi^2$	Mo(^{5}G) + S(^{3}P)	2.7	Mo(^{5}D) + S(^{3}P)
$^7\Pi$	$\frac{0.99}{\sqrt{2}}\left\|1\sigma^2 2\sigma^2 3\sigma^1\left(1\pi_x^1 2\pi_x^1 1\pi_y^2 2\pi_y^1 + 1\pi_x^2 2\pi_x^1 1\pi_y^1 2\pi_y^1\right)1\delta_+^1 2\delta_-^1\right\rangle$	σ^2	Mo(^{7}S) + S(^{3}P)	-	Mo(^{7}S) + S(^{3}P)
$^3\Pi$	$\frac{0.84}{\sqrt{2}}\|1\sigma^2 2\sigma^2 3\sigma^1\left(1\pi_x^2 1\pi_y^2 2\bar{\pi}_y^1 + 1\pi_x^2 2\bar{\pi}_x^1 1\pi_y^2\right)1\delta_+^1 2\delta_-^1\rangle$	$\sigma^2\pi^2$	Mo(^{5}S) + S(^{3}P)	-	Mo(^{5}S) + S(^{3}P)
$^5\Delta$	$\frac{0.90}{\sqrt{2}}\|1\sigma^2 2\sigma^2 1\pi_x^2 2\pi_x^1 1\pi_y^2 2\pi_y^1(1\delta_+^1 + 1\delta_-^1)\rangle$	$\sigma^2\pi^2\pi^2$	Mo(^{5}D) + S(^{1}D)	2.7	Mo(^{5}D) + S(^{3}P)
$^7\Sigma^+$	$0.99\left\|1\sigma^2 2\sigma^1 3\sigma^1 1\pi_x^2 2\pi_x^1 1\pi_y^2 2\pi_y^1 1\delta_+^1 1\delta_-^1\right\rangle)$	σ^1	Mo(^{7}S) + S(^{1}D)	-	Mo(^{7}S) + S(^{1}D)
$^5\Pi(2)$	$\frac{0.75}{\sqrt{2}}\left\|1\sigma^2 2\sigma^2 3\sigma^1(1\pi_x^1 2\bar{\pi}_x^1 1\pi_y^2 2\pi_y^1 + 1\pi_x^2 2\pi_x^1 1\pi_y^1 2\bar{\pi}_y^1)1\delta_+^1 1\delta_-^1\right\rangle)$	σ^2	Mo(^{5}S) + S(^{3}P)	-	Mo(^{5}S) + S(^{3}P)
$^3\Sigma^+$	$0.44\|1\sigma^2 2\sigma^2(1\pi_x^2 2\pi_x^1 1\pi_y^2 2\bar{\pi}_y^1 + 1\pi_x^2 2\bar{\pi}_x^1 1\pi_y^2 2\pi_y^1)(1\delta_+^1 1\bar{\delta}_-^1 + 1\bar{\delta}_+^1 1\delta_-^1)\rangle$	$\sigma^2\pi^2\pi^2$	Mo(^{5}D) + S(^{1}D)	3.0	Mo(^{5}D) + S(^{3}P)
$^3\Delta(2)$	$0.49\|1\sigma^2 2\sigma^2(1\pi_x^2 2\pi_x^1 1\pi_y^2 2\bar{\pi}_y^1 - 1\pi_x^2 2\bar{\pi}_x^1 1\pi_y^2 2\pi_y^1)(1\delta_+^1 1\bar{\delta}_-^1 + 1\bar{\delta}_+^1 1\delta_-^1)\rangle$	$\sigma^2\pi^2\pi^2$	Mo(^{5}D) + S(^{1}D)	2.6	Mo(^{5}D) + S(^{3}P)
$^7\Sigma^-$	$0.63\|1\sigma^2 2\sigma^2 3\sigma^1 4\sigma^1\left(1\pi_x^1 2\pi_x^1 1\pi_y^2 + 1\pi_x^2 1\pi_y^1 2\pi_y^1\right)1\delta_+^1 1\delta_-^1\rangle$	π^2	Mo(^{7}S) + S(^{3}P)	-	Mo(^{7}S) + S(^{3}P)
$^7\Delta$	$\frac{0.70}{\sqrt{2}}\|1\sigma^2 2\sigma^2 3\sigma^1 4\sigma^1(1\pi_x^1 1\pi_y^2 2\pi_y^1 - 1\pi_x^2 2\pi_x^1 1\pi_y^1 + 1\pi_x^1 2\pi_x^1 1\pi_y^2 - 1\pi_x^2 1\pi_y^1 2\pi_y^1)1\delta_+^1 1\delta_-^1\rangle)$	π^1	Mo(^{7}S) + S(^{1}D)	-	Mo(^{7}S) + S(^{1}D)
$^5\Sigma^-(2)$	$0.54\|1\sigma^2 2\sigma^2 3\sigma^2\left(1\pi_x^1 2\pi_x^1 1\pi_y^2 + 1\pi_x^2 1\pi_y^1 2\pi_y^1\right)1\delta_+^1 1\delta_-^1\rangle$	$\sigma^2\pi^2$	Mo(^{5}D) + S(^{3}P)	3.0	Mo(^{5}S) + S(^{3}P)
$^7\Pi(2)$	$\frac{0.90}{\sqrt{2}}\left\|1\sigma^2 2\sigma^2 3\sigma^1\left(1\pi_x^1 2\pi_x^1 1\pi_y^2 2\pi_y^1 + 1\pi_x^2 2\pi_x^1 1\pi_y^1 2\pi_y^1\right)1\delta_+^1 1\delta_-^1\right\rangle)$	σ^2	Mo(^{5}S) + S(^{3}P)	2.9	Mo(^{7}S) + S(^{1}D)
$^7\Pi(3)$	$\frac{0.70}{\sqrt{2}}\|1\sigma^2 2\sigma^2 3\sigma^1(1\pi_x^2 2\pi_x^1 1\pi_y^1 2\pi_y^1 - 1\pi_x^1 2\pi_x^1 1\pi_y^2 2\pi_y^1)(1\delta_+^1 + 1\delta_-^1)\rangle)$	σ^2	Mo(^{7}S) + S(^{1}D)	2.9	Mo(^{5}S) + S(^{3}P)
$^9\Sigma^-$	$0.99\|1\sigma^2 2\sigma^2 3\sigma^1 4\sigma^1 1\pi_x^1 2\pi_x^1 1\pi_y^1 2\pi_y^1 1\delta_+^1 1\delta_-^1\rangle$	-	-	-	Mo(^{7}S) + S(^{3}P)
$^9\Pi$	$\frac{0.99}{\sqrt{2}}\|1\sigma^2 2\sigma^2 3\sigma^1 4\sigma^1\left(1\pi_x^1 2\pi_x^1 1\pi_y^2 2\pi_y^1 + 1\pi_x^2 2\pi_x^1 1\pi_y^1 2\pi_y^1\right)1\delta_+^1 1\delta_-^1\rangle)$	-	-	-	Mo(^{7}S) + S(^{3}P)
$^7\Sigma^-(2)$	$0.99\|1\sigma^2 2\sigma^2 3\sigma^1 4\bar{\sigma}^1 1\pi_x^1 2\pi_x^1 1\pi_y^1 2\pi_y^1 1\delta_+^1 1\delta_-^1\rangle$	-	-	-	Mo(^{5}S) + S(^{3}P)

[a] Mo (^{7}S, 5s^{1}4d^5); Mo (^{5}S, 5s^{1}4d^5); Mo (^{5}D, 5s^{2}4d^4); Mo(^{5}G, 5s^{2}4d^4) ; S (^{3}P, 3s^{2}3p^4); S (^{1}D, 3s^{2}3p^4).

Table 3. Bond distances r_e (Å), Dissociation energies D_e (eV) and corrected values for zero-point energy D_0 (eV), and Harmonic Frequencies ω_e (cm^{-1}), of the $X^5\Pi$ state at RCCSD(T), RCCSD[T]/aug-cc-CV*5*Z-PP_{Mo}/aug-cc-CV*5*Z_S, and C-RCCSD(T), RCCSD[T]/aug-cc-pwCV*5*Z-PP_{Mo} /aug-cc-pwCV*5*Z_S.

	aug-cc-pV5Z(-PP_{Mo})		**aug-cc-pwCV5Z(-PP_{Mo})**	
	RCCSD(T)	**RCCSD[T]**	**C-RCCSD(T)**	**C-RCCSD[T]**
r_e	2.1313	2.1461	2.1161	2.1337
D_e	3.705	3.863	3.757	3.937
D_0	3.674	3.834	3.725	3.907
ω_e	508.7	480.9	513.0	490.8

Table 4. Bond distances r_e (Å), Dissociation energies D_e (eV), Dissociation energies corrected for zero-point energy D_0 (eV), and Harmonic Frequencies ω_e (cm^{-1}), of the $X^5\Pi$ state at C-RCCSD(T) and C-RCCSD[T]/ aug-cc-pwCV*x*Z-PP_{Mo} /aug-cc-pwCV*x*Z_S, where *x* = D, T, Q, and 5.

	C-RCCSD(T)/aug-cc-pwCVxZ(-PP_{Mo})					**C-RCCSD[T]/aug-cc-pwCVxZ(-PP_{Mo})**					**Expt**
	x = D	*x = T*	*x = Q*	*x = 5*	CBS-limit[a]	*x = D*	*x = T*	*x = Q*	*x = 5*	CBS-limit[a]	
r_e	2.1455	2.1266	2.1187	2.1161	2.114±0.0005	2.1673	2.1461	2.1365	2.1337	2.131±0.001	
D_e	3.300	3.574	3.707	3.757	3.81±0.01	3.498	3.759	3.886	3.937	3.99±0.01	
D_0	3.269	3.542	3.675	3.725	3.78±0.01	3.469	3.730	3.856	3.907	3.956±0.009	3.932±0.004
ω_e	500.7	511.2	513.4	513.0	513.4±0.4	465.6	479.7	487.6	490.8	494.8±1.2	

[a] Extrapolation to the CBS limit using the equation (1).

Table 5. CBS limits of Dissociation energies D_e (eV) and Dissociation energies corrected for zero-point energy D_0 (eV) of the $X^5\Pi$ state at C-RCCSD(T) and C-RCCSD[T].

		C-RCCSD(T)		C-RCCSD[T]	
		D_e	**D_0**	**D_e**	**D_0**
$y_x = y_{CBS} + A\ e^{-Bx}$	I[a]	3.81±0.01	3.78±0.01	3.99±0.01	3.956±0.009
$y_x = y_{CBS} + A\ e^{-Bx}$	II[b]	3.788	3.756	3.971	3.940
$y_x = y_{CBS} + A\ e^{-(x-1)} + B\ e^{-(x-1)^2}$	II[b]	3.786	3.755	3.967	3.936
$y_x = y_{CBS} + Ax^{-b}$	II[b]	3.812	3.780	3.998	3.967
Expt			3.932±0.004		3.932±0.004

[a] Approach I: The dissociation energies are calculated in a series of basis sets and then these obtained values are extrapolated using exponential formula.

[b] Approach II: Total energies, for n = T, Q, 5, are extrapolated to the CBS limit and then the dissociation energies are calculated for the extrapolated CBS PEC.

Table 6. Final Bond Lengths r_e (Å), Dissociation Energies D_e (eV), corrected values with respect to the zero-point energy, D_0 (eV), and the corresponding diabatic values D_e^d and D_0^d.

State	r_e	D_e	D_e^d	D_0	D_0^d
$X^5\Pi$	2.131	3.99		3.96	
$^3\Sigma^-$	2.054	4.72	5.08	4.68	5.05
$^5\Sigma^-$	2.145	2.92		2.90	
$^5\Sigma^+$	2.174	4.65	5.77	4.62	5.74
$^3\Delta$	2.071	4.61	5.00	4.58	4.96
$^7\Pi$	2.407	2.68		2.66	
$^3\Pi$	2.107	4.16		4.13	
$^5\Delta$	2.147	4.19	5.31	4.16	5.28
$^7\Sigma^+$	2.359	2.84		2.82	
$^5\Pi(2)$	2.326	3.04		3.01	
$^3\Sigma^+$	2.163	3.32	4.43	3.29	4.40
$^3\Delta(2)$	2.179	3.36	4.48	3.33	4.45
$^7\Sigma^-$	2.378	1.39		1.36	
$^7\Delta$	2.434	2.28		2.26	
$^5\Sigma^-(2)$	2.290	2.60	2.96	2.57	2.94
$^7\Pi(2)$	2.521	2.18	2.39	2.16	2.37

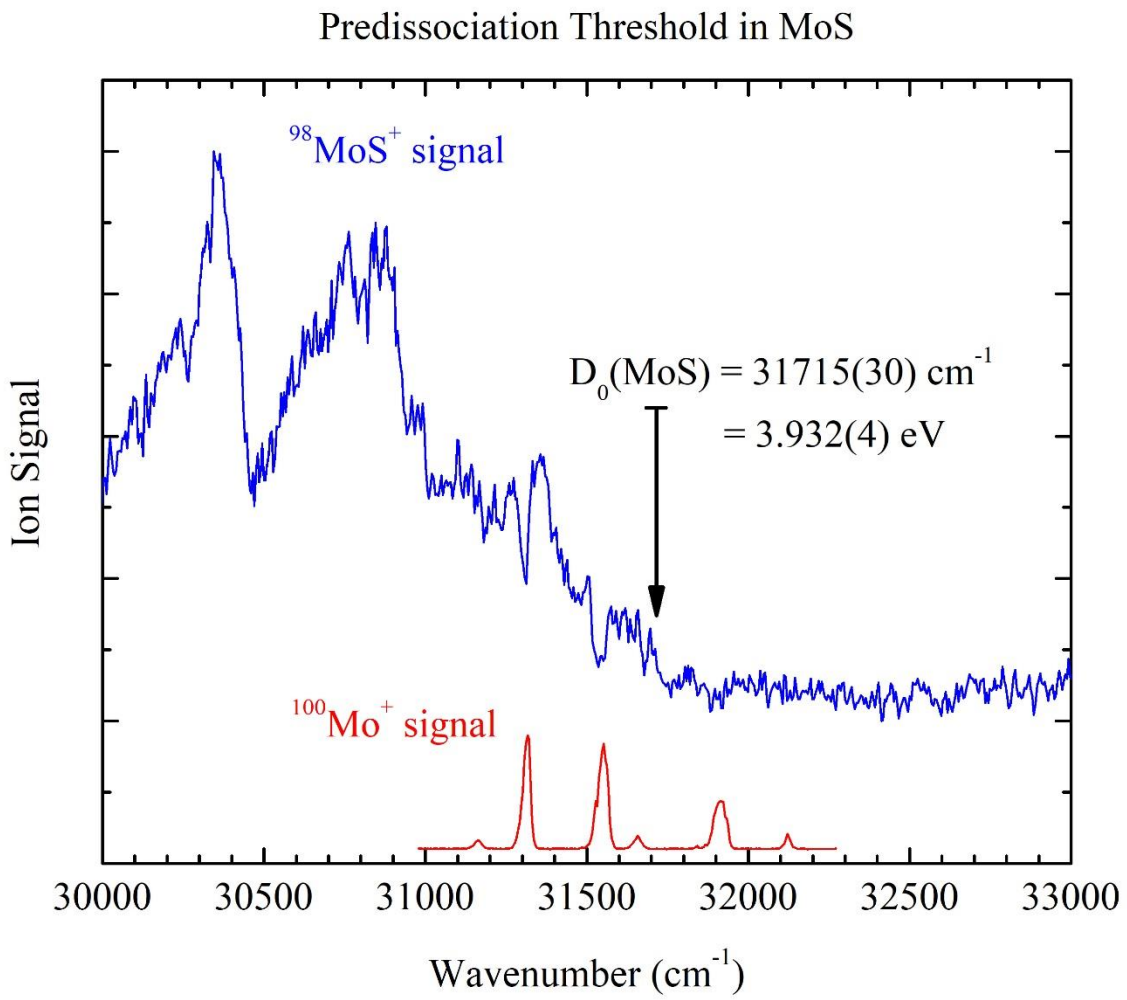

Figure 1. The R2PI spectrum of MoS (upper blue trace) in the energetic vicinity of its predissociation threshold located at 31715(30) cm^{-1}. Mo atomic transitions (lower red trace) were used to calibrate the spectrum.

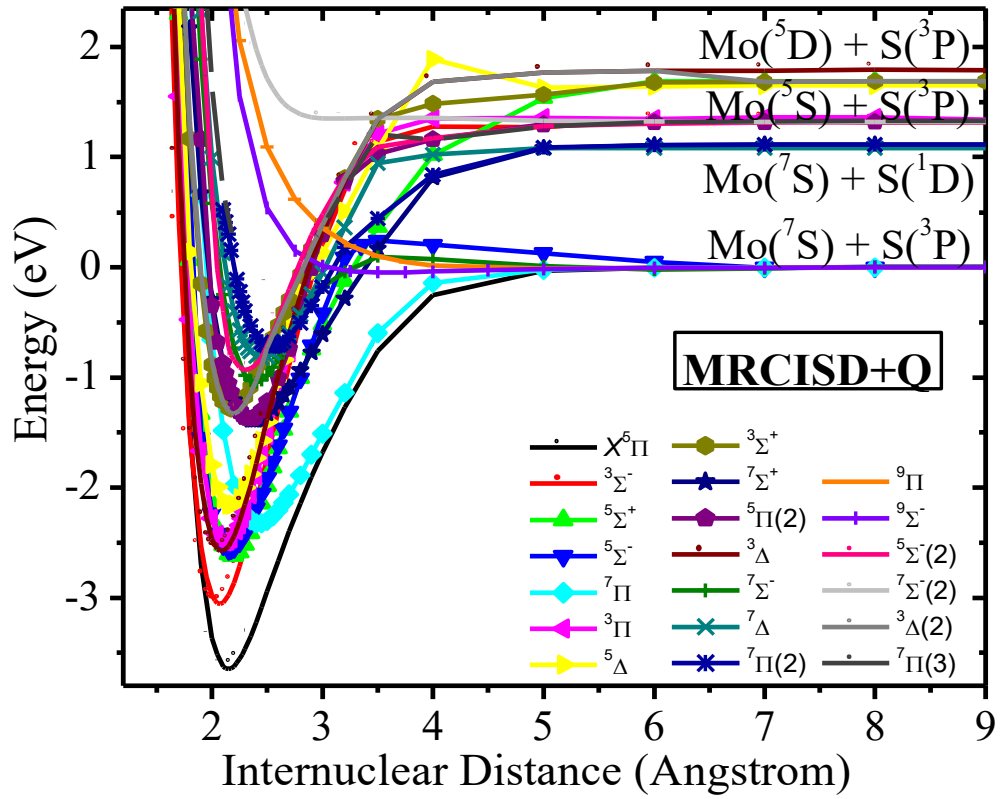

Figure 2. PECs of the twenty calculated states of MoS at the MRCISD+Q/aug-cc-pV5Z(-PP_{Mo}) level of theory.

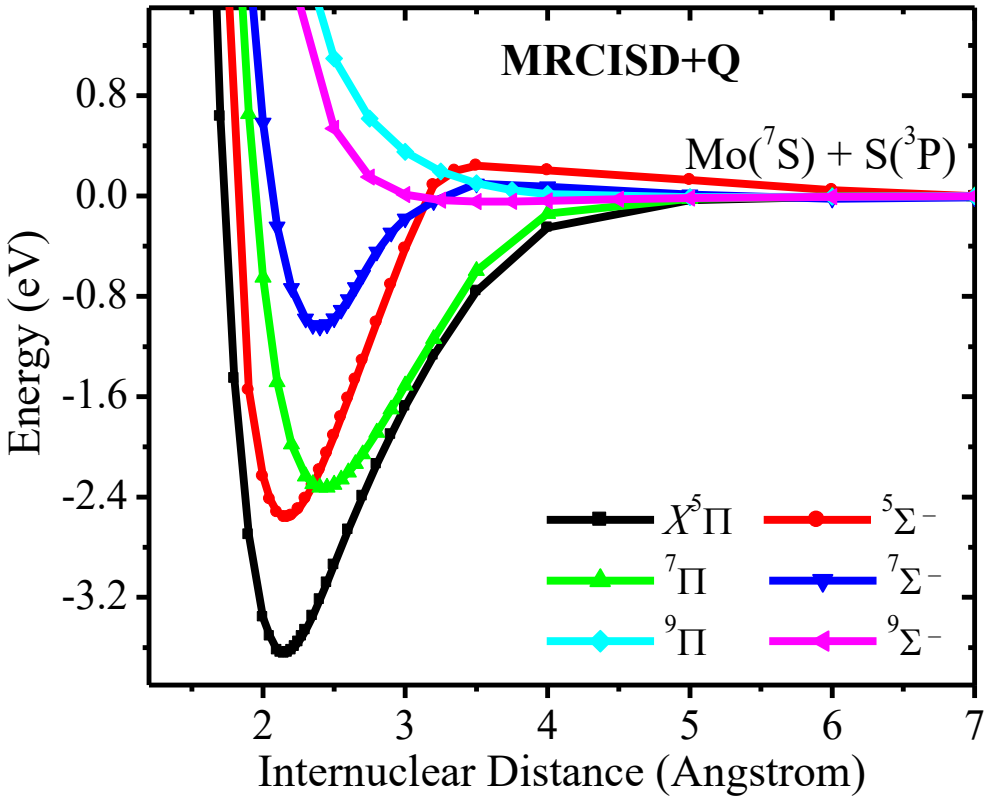

Figure 3. PECs of the six states of MoS, which correlate to the atomic ground state products at the MRCISD+Q/aug-cc-pV5Z(-PP_{Mo}) level of theory.

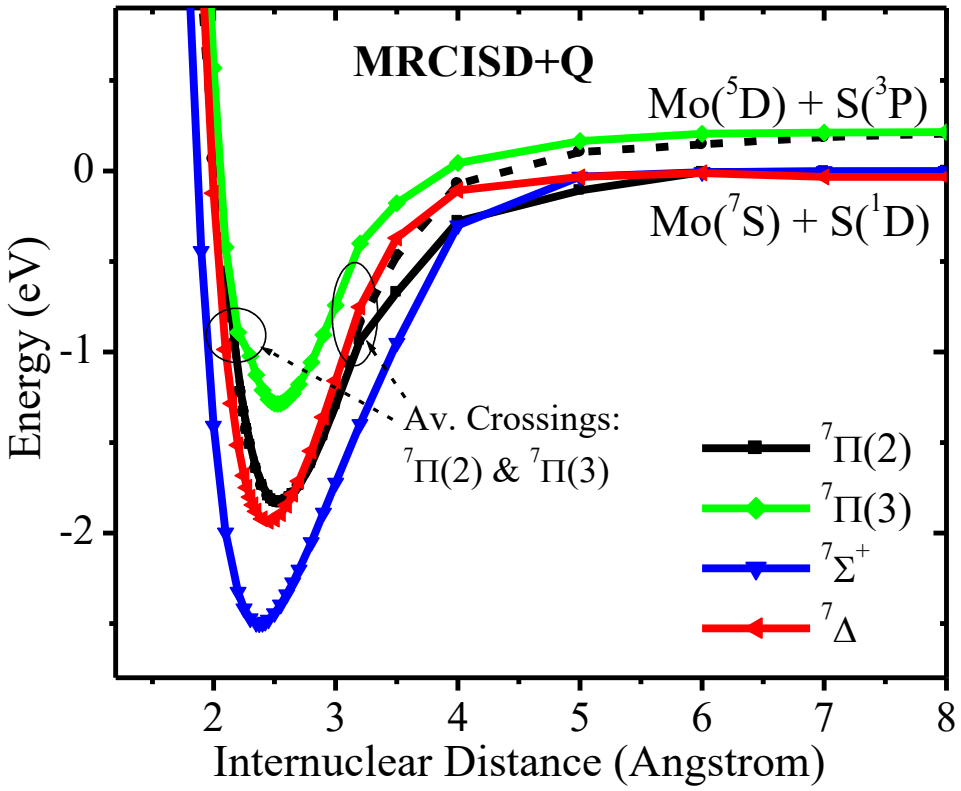

Figure 4. PECs of the three states of MoS, which correlate to the Mo(^{7}S) + S(^{1}D) atomic state products and of $^7\Pi(3)$ which present avoided crossing with $^7\Pi(2)$ at MRCISD+Q/aug-cc-pV5Z(-PP$_{Mo}$). (Dot line corresponds to diabatic PEC of $^7\Pi(2)$.

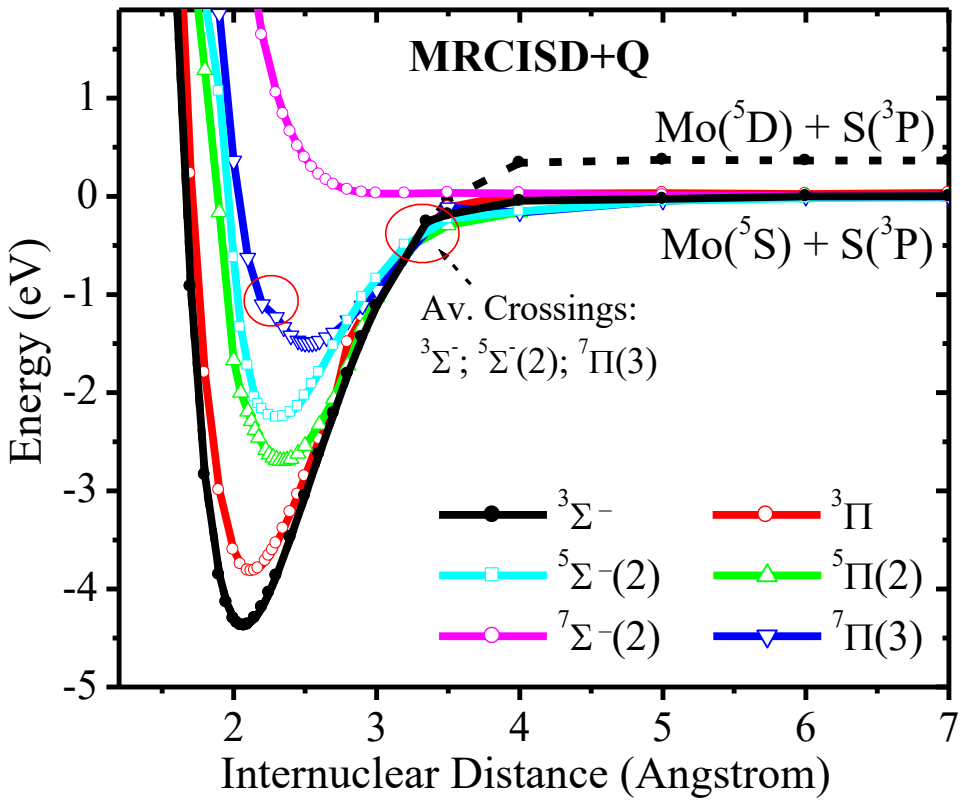

Figure 5. PECs of the calculated states of MoS, which correlate to the Mo(^{5}S) + S(^{3}P) atomic state products at MRCISD+Q/aug-cc-pV5Z(-PP$_{Mo}$). (Dot line corresponds to diabatic PEC)

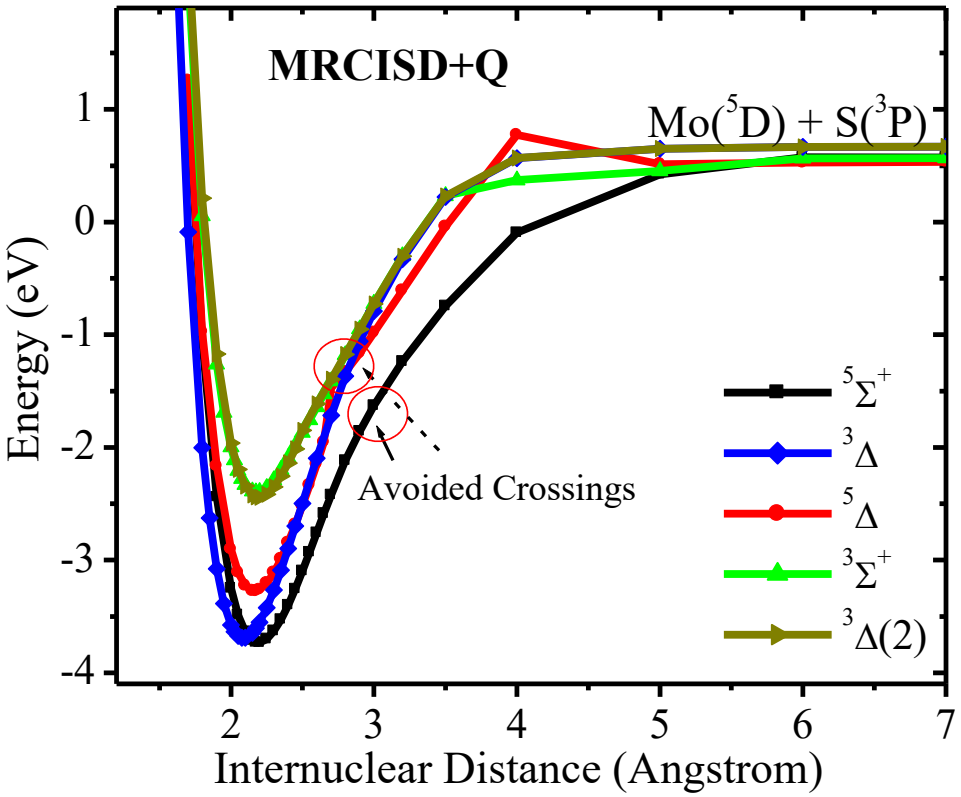

Figure 6. PECs of the calculated states of MoS, which correlate to the Mo(^{5}D) + S(^{3}P) atomic state products at MRCISD+Q/aug-cc-pV5Z(-PP$_{Mo}$).

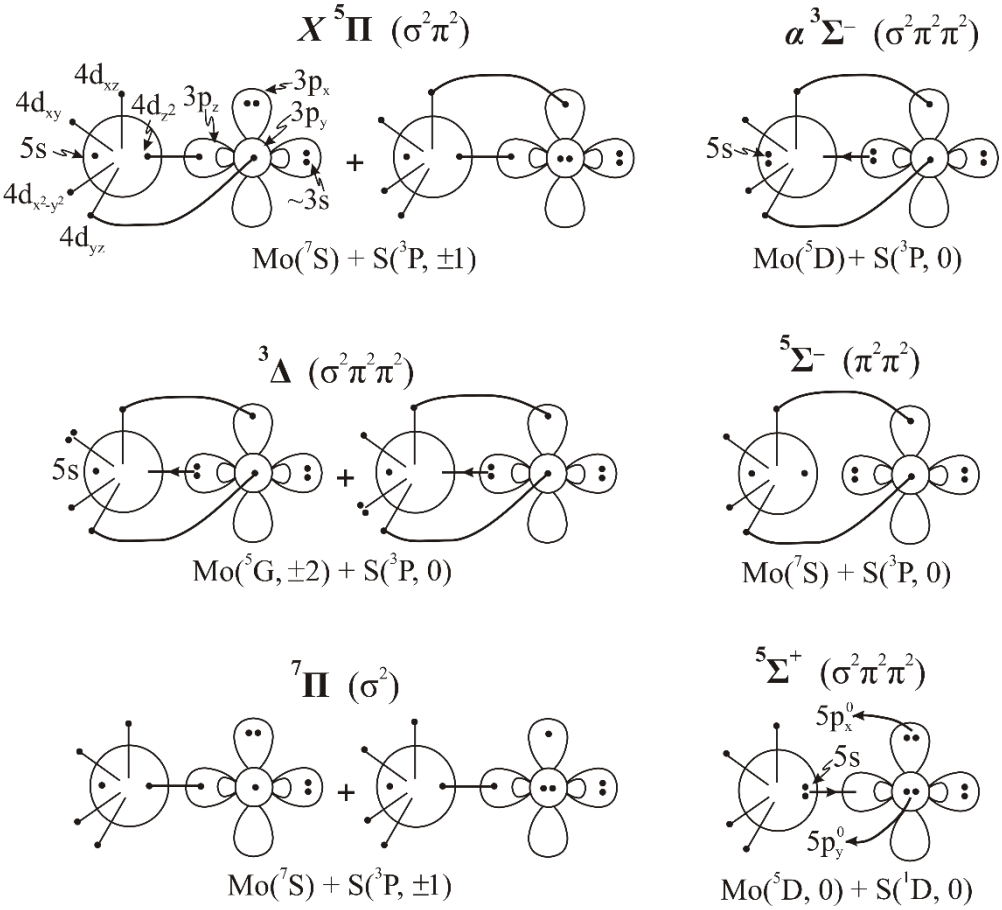

Scheme 1: vbL bonding icons of the $X^3\Pi$, $a^3\Sigma^-$, $A^5\Sigma^-$, $^3\Delta$, $^7\Pi$, and $^5\Sigma^+$ states.

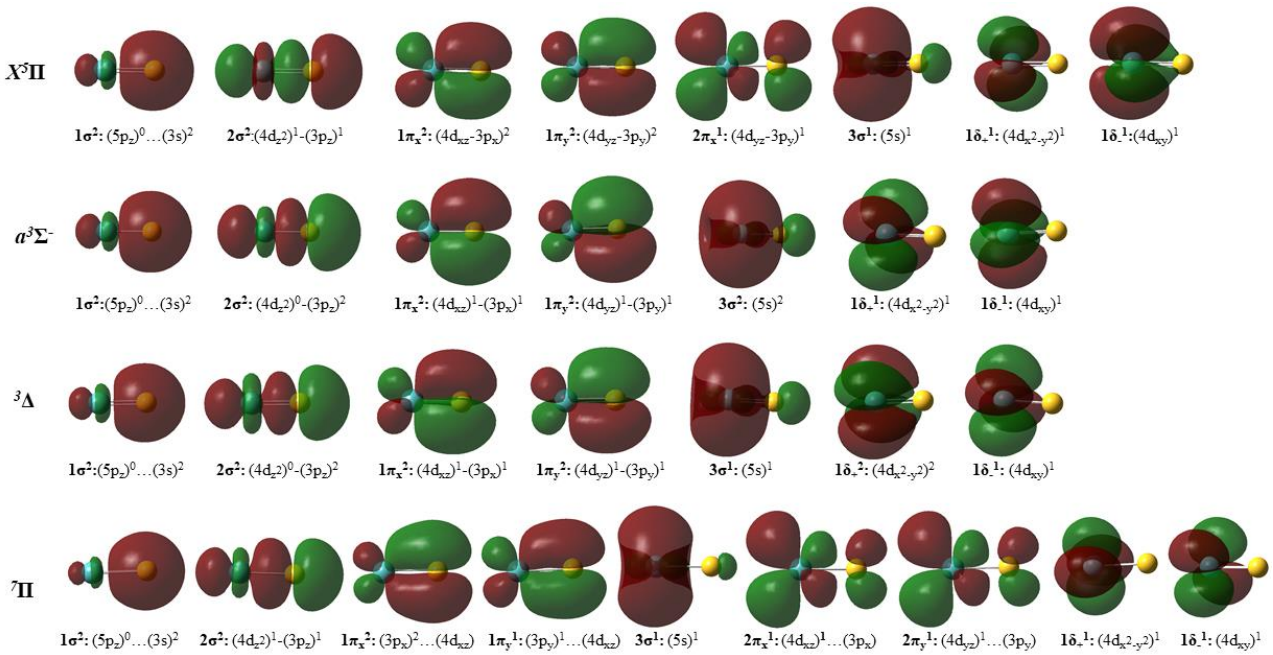

Figure 7: Molecular orbitals of the $X^3\Pi$, $\alpha^3\Sigma^-$, $^3\Delta$, and $^7\Pi$ states. The atomic orbitals with the main contribution are given for each MO.

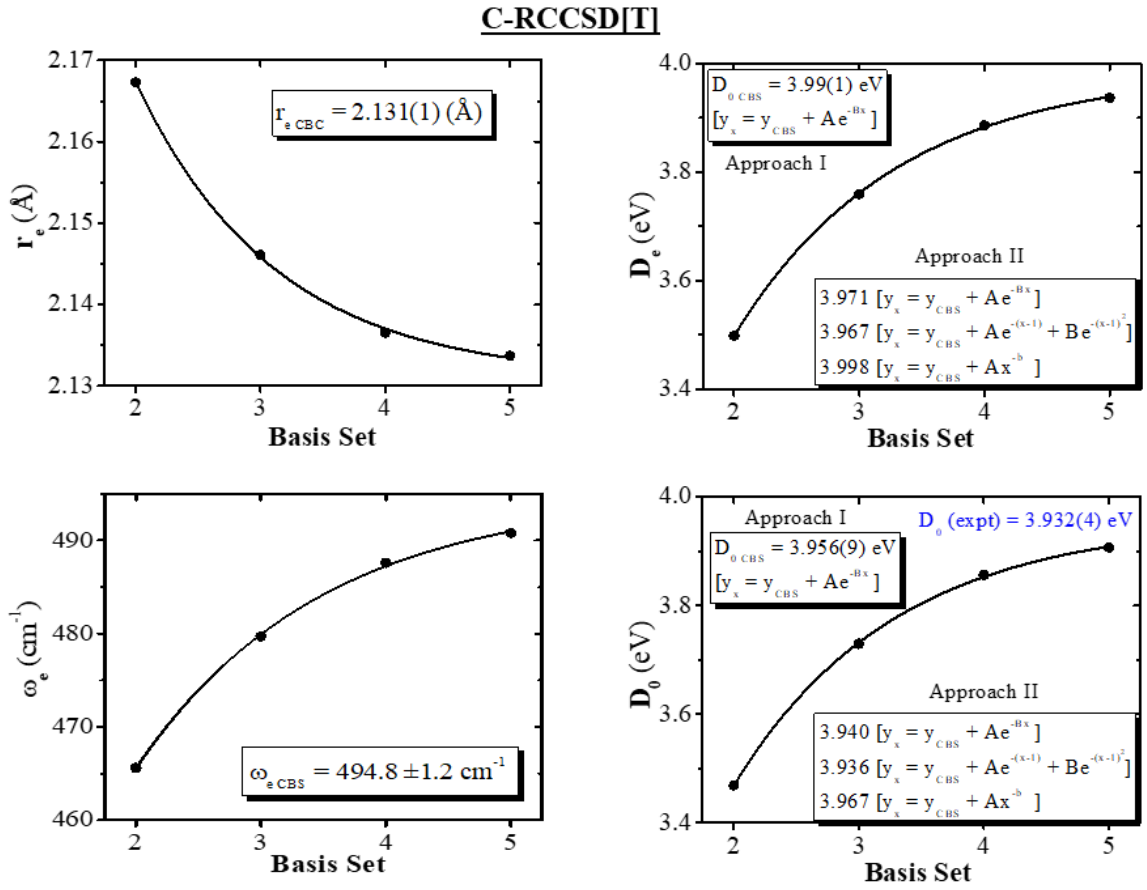

Figure 8. C-RCCSD[T] Bond distances R_e, Dissociation energies D_e, Dissociation energies corrected for zero-point energy D_0, and Harmonic Frequencies ω_e, with respect to the basis set size, aug-cc-pwCV*x*Z-PP$_{Mo}$ /aug-cc-pwCV*x*Z$_S$, *x* = D(2), T(3), Q(4), 5.

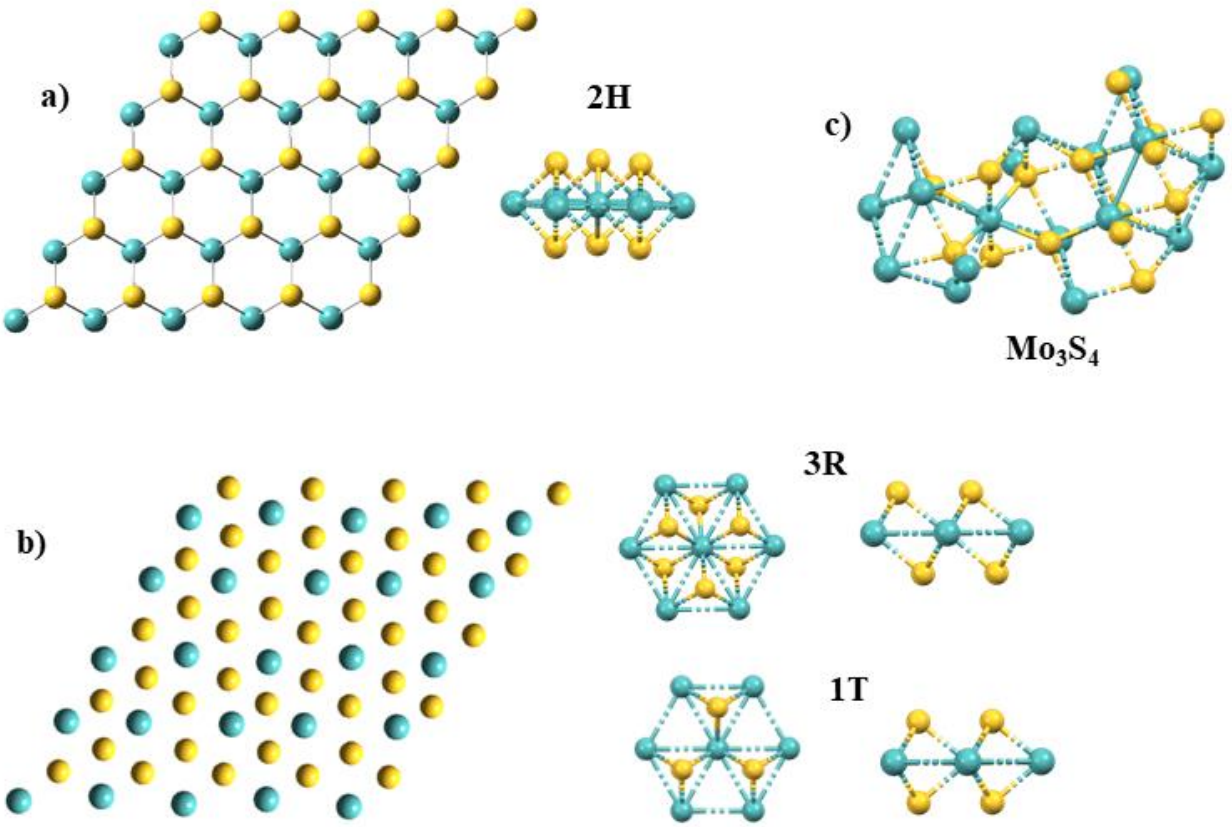

Figure 9. Top and side views of **a)** 2H, **b)** 1T and 3R, and **c)** Mo_3S_4 polymorphs.

TOC Graphic

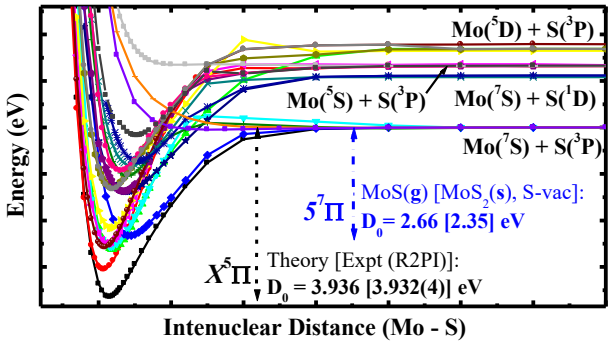
Mo(5D) + S(3P)
Mo(5S) + S(3P)
Mo(7S) + S(1D)
Mo(7S) + S(3P)
5 7Π
MoS(g) [MoS2(s), S-vac]:
D0 = 2.66 [2.35] eV
X 5Π
Theory [Expt (R2PI)]:
D0 = 3.936 [3.932(4)] eV
Energy (eV)
Intenuclear Distance (Mo - S)